J. Fluid Mech. (2000), *vol.* 421, *pp.* 83–114. Printed in the United Kingdom

The dynamics of two-layer gravity-driven flows in permeable rock

By ANDREW W. WOODS[1] AND ROBERT MASON[2]

[1]BP Institute for Multiphase Flow, Madingley Road, University of Cambridge, Cambridge CB3 OEZ, UK

[2]Centre for Environmental and Geophysical Flows, School of Mathematics, University of Bristol, Bristol, BS8 1TW, UK

(Received 2 July 1999 and in revised form 25 April 2000)

We examine the motion of a two-layer gravity current, composed of two fluids of different viscosity and density, as it propagates through a model porous layer. We focus on two specific situations: first, the case in which each layer of fluid has finite volume, and secondly, the case in which each layer is supplied by a steady maintained flux. In both cases, we find similarity solutions which describe the evolution of the flow. These solutions illustrate how the morphology of the interface between the two layers of fluid depends on the viscosity, density and volume ratios of the two layers. We show that in the special case that the viscosity ratio of the upper to lower layers, V, satisfies $V = (1 + F)/(1 + RF)$ where F and R are respectively the ratios of the volume and buoyancy of the lower layer to those of the upper layer, then the ratio of layer depths is the same at all points. Furthermore, we show that for $V > (<)(1 + F)/(1 + RF)$, the lower (upper) layer advances ahead of the upper (lower) layer. We also present some new laboratory experiments on two-layer gravity currents, using a Hele-Shaw cell, and show that these are in accord with the model predictions. One interesting prediction of the model, which is confirmed by the experiments, is that for a finite volume release, if the viscosity ratio is sufficiently large, then the less-viscous layer separates from the source. We extend the model to describe the propagation of a layer of fluid which is continuously stratified in either density or viscosity, and we briefly discuss application of the results for modelling various two-layer gravity-driven flows in permeable rock.

1. Introduction

The displacement of one fluid by a second through a porous layer is a central process in many natural and industrial flows through porous layers. It is of especial interest for the oil industry in which polymer-rich water or gas may be injected into an oil field to enhance oil recovery (Gorell & Homsy 1983). The phenomenon is also relevant for groundwater remediation when liquid may be injected to contain or disperse contaminants present in aquifers (Zhou & Blunt 1997). A related process in the geothermal industry involves the injection of liquid to stimulate heat recovery from hot rock (Woods 1999). There is a considerable literature on displacement flows in porous rocks (e.g. Bear 1972; Homsy 1987; Manickam & Homsy 1993; Zimmerman & Homsy 1991; Tchelepi & Orr 1993). As well as the effects of capillarity and wetting (e.g. Dullien 1992), a particular focus of such work has been the development of understanding of the viscous fingering instability in a purely pressure-driven flow

(Saffman & Taylor 1958; Chouke, Moers & van der Poel 1959; Homsy 1987). This instability arises when fluid of low viscosity displaces fluid of greater viscosity thereby leading to an adverse pressure gradient across the interface. Much attention has focused on modelling the nonlinear evolution of the finger zone which develops following the initial instability. In a purely pressure-driven flow through a porous layer, this region tends to grow with time, producing a region in which the two fluids are intricately interleaved (Homsy 1987).

In many of the above displacement flows, the two fluids often have different density as well as viscosity. As a result, even with no applied pressure, the buoyancy forces lead to relative motions between the two layers as they spread under gravity through the porous layer. There have been a number of numerical calculations of the macroscopic behaviour of displacement flows involving viscous instability, permeability heterogeneity and gravity in three dimensions (e.g. Tchelepi & Orr 1993); also, some experiments on miscible displacement flows have been carried out in model porous layers consisting of packed glass balls, using aqueous saline solutions (e.g. Peters, Zhou & Blunt 1997). A primary focus of those experiments was to examine the effect of the competition between the gravitational force and the applied pressure gradient on recovery rates. Motivated by the richness and complexity of such flows, here we report on a fundamental theoretical and experimental study of the dynamics of purely gravitationally driven two-layer flow composed of fluid layers of different viscosity and density.

We investigate the propagation of the two fluid layers along a horizontal, impermeable boundary of a porous layer. The porous layer is assumed to be saturated with a deep layer of a third fluid of smaller density (e.g. air/gas) which is dynamically inactive. For simplicity we neglect effects of melting and capillarity, and assume the interface remains sharp; this is in accord with our experiments on miscible displacement in a Hele-Shaw cell (§ 4), but is an idealization for flow in a porous layer. We examine the rate of migration of the two fluid layers as a function of their buoyancy and viscosity contrast. We also predict the nonlinear shape of each layer and the interface between the layers. The structure of this interface may be interpreted as a gravity-driven viscous finger, and is complementary to the nonlinear, purely pressure-driven solutions derived by Saffman & Taylor (1958). We compare the predictions of our model with a series of laboratory experiments in a Hele-Shaw cell. These confirm our predictions of the important control that the viscosity contrast, as well as the buoyancy contrast, has on the structure of the flow.

In § 2 we develop a model of a two-layer gravity current and we identify the boundary conditions across the interface between the two fluids. We then examine how the interface morphology varies when a finite mass of each fluid is released at the source (§ 3). These theoretical predictions are successfully compared with a series of new laboratory experiments in § 4, and the model is extended to describe the evolution of a two-layer current produced by a steady flux released at the source (§ 5). In § 6, we extend the model to describe the release of a fluid which is continuously stratifed in either density or viscosity and we draw some conclusions in § 7.

2. The model of a two-layer gravity current

We consider a two-layer gravity current propagating along a horizontal lower boundary through a porous layer of permeability k filled with fluid of density ρ. We assume that the volume of fluid in each of the layers, i, is given by $Q_i t^\gamma$ where $i = u, l$ represent the upper and lower layer respectively. The case $\gamma = 0$ corresponds to a

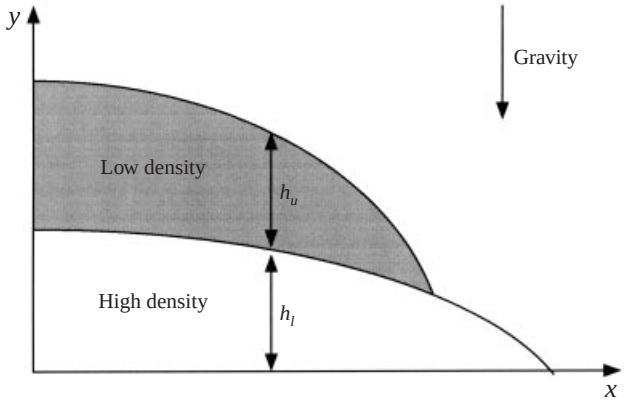

FIGURE 1. Schematic of the motion of a two-layer gravity current, showing some of the variables used in the text.

finite release at $t = 0$, and $\gamma = 1$ corresponds to a maintained steady release. We consider the flow to be subject to Darcy's law and assume that the interface between the fluids remains sharp as is approximately the case in our Hele-Shaw experiments. Let us denote the density, viscosity and depth of each of the two layers in the current as having values $\rho + \Delta\rho_i$, μ_i and h_i (figure 1). Once the two-layer current has become long and thin, the pressure gradient is approximately hydrostatic (Barenblatt 1996) and

$$p(y) = p_H + \rho g(H - y) + \Delta\rho_u g(h_u + h_l - y) \quad \text{for} \quad h_u + h_l > y > h_l \tag{2.1}$$

while

$$p(y) = p_H + \rho g(H - y) + \Delta\rho_l g(h_l - y) + \Delta\rho_u g h_u \quad \text{for} \quad h_l > y > 0, \tag{2.2}$$

where H and p_H are the height and pressure at some reference point above both the layers. In this geometry, the gravitational acceleration is directed in the $-y$-direction. In this limit, the horizontal Darcy velocity in the upper layer is

$$u_u = -\frac{k}{\mu_u}\Delta\rho_u g\left(\frac{\partial h_l}{\partial x} + \frac{\partial h_u}{\partial x}\right) \tag{2.3}$$

while the Darcy velocity in the lower layer has value

$$u_l = -\frac{k}{\mu_l}\left(\Delta\rho_l g\frac{\partial h_l}{\partial x} + \Delta\rho_u\frac{\partial h_u}{\partial x}\right), \tag{2.4}$$

where k is the permeability of the porous rock. The conservation of mass in each layer, denoted by $i = u, l$ for upper and lower layers respectively, satisfies

$$\phi\frac{\partial h_i}{\partial t} + \frac{\partial h_i u_i}{\partial x} = 0 \tag{2.5}$$

in terms of the porosity, ϕ, of the matrix. If we define the characteristic flow speed

$$S = \frac{kg\Delta\rho_u}{\phi\mu_u} \tag{2.6}$$

and the viscosity and buoyancy ratios

$$V = \mu_u/\mu_l \quad \text{and} \quad R = \frac{\Delta\rho_l}{\Delta\rho_u} \tag{2.7}$$

then the equations governing the depth of each of the two layers of fluid are

$$\frac{\partial h_l}{\partial t} = SV\frac{\partial}{\partial x}\left(h_l\left(\frac{\partial h_u}{\partial x} + R\frac{\partial h_l}{\partial x}\right)\right) \tag{2.8}$$

and

$$\frac{\partial h_u}{\partial t} = S\frac{\partial}{\partial x}\left(h_u\left(\frac{\partial h_l}{\partial x} + \frac{\partial h_u}{\partial x}\right)\right). \tag{2.9}$$

The global conservation of mass for each layer has the form

$$Q_i t^\gamma = \phi\int_{L_{i1}}^{L_{i2}} h_i\,\mathrm{d}x \tag{2.10}$$

for each layer, where L_{i1} and L_{i2} denote the location of the leading and trailing edge of fluid i. We define the ratio of volumes of the two layers by

$$F = Q_l/Q_u. \tag{2.11}$$

To complete the problem, we now specify the boundary conditions.

Source conditions ($x = 0$)*:* If $\gamma > 0$, so that fluid continues to be supplied to each layer, then conservation of flux at the origin requires

$$(hu)_i|_{x=0} = \gamma Q_i t^{\gamma-1}. \tag{2.12}$$

However, in the special case $\gamma = 0$, there is zero flux at the origin and two situations may develop. Both layers may remain attached to the origin, in which case

$$\frac{\partial h_i}{\partial x}(0) = 0 \tag{2.13}$$

for both layers. Alternatively, only one layer may remain attached to the source, in which case for that layer $\partial h_i/\partial x|_0 = 0$. In the other layer, which detaches from the source, the layer depth remains equal to zero up to some point L_{j0} say, so that $h_j = 0$ for $0 \leqslant x \leqslant L_{j0}$ say.

Leading edge: We denote the lateral extent of the shorter of the two layers, i say, to have value L_i, so that at the point $x = L_i$, $h_i(L_i) = 0$. In the more extensive layer, j say,

$$[h_j]_{L_i-}^{L_i+} = 0 \quad \text{and} \quad [u_j]_{L_i-}^{L_i+} = 0. \tag{2.14}$$

In the region ahead of the shorter layer, the flow behaves as a single-layer gravity current

$$\frac{\partial h_j}{\partial t} = S_j\frac{\partial}{\partial t}\left(h_j\frac{\partial h_j}{\partial t}\right), \tag{2.15}$$

where $S_j = S$ if $j = u$ and $S_j = SVR$ if $j = l$.

In the next three sections, we describe similarity solutions for this model system, corresponding to a finite release of fluid in each layer, $\gamma = 0$ (§ 3), and a fixed flux of fluid in each layer, $\gamma = 1$ (§ 5). By comparison with new laboratory experiments (§ 4), we show that these similarity solutions represent the long-time asymptotic solution to which the currents evolve once the aspect ratio (length/height) of each layer increases beyond values of order 10.

3. Finite release of fluid

For a single-layer current there is an analytic similarity solution in the case of a finite release of fluid, $\gamma = 0$ (Pattle 1959; Barenblatt 1996) which agrees well with

laboratory experiments (Huppert & Woods 1995). The solution predicts that the current depth $h(x,t)$ has the form

$$h = \frac{1}{6}\left(\frac{Q^2}{St}\right)^{1/3}\left(\left(\frac{9}{\phi}\right)^{2/3} - \frac{x^2}{(QSt)^{2/3}}\right). \tag{3.1}$$

The present problem involves two layers, but the solution (3.1) suggests dimensionless scalings for the depth and extent of each layer in terms of the volume of fluid in the upper layer, Q_u, the natural speed S, the porosity ϕ and the time t. We therefore introduce the similarity variable

$$\eta = x/H(\omega t)^{1/3} \tag{3.2}$$

and the similarity scalings for each current

$$h_u = H(\omega t)^{-1/3} f_u(\eta) \quad \text{and} \quad h_l = H(\omega t)^{-1/3} f_l(\eta), \tag{3.3}$$

with $H = (Q_u/\phi)^{1/2}$ and $\omega = S/(Q_u/\phi)^{1/2}$. Equations (2.8), (2.9) may then be reduced to the self-similar equations

$$-\frac{\mathrm{d}(\eta f_u)}{\mathrm{d}\eta} = 3\frac{\mathrm{d}}{\mathrm{d}\eta}\left[f_u\frac{\mathrm{d}}{\mathrm{d}\eta}(f_u + f_l)\right] \tag{3.4}$$

and

$$-\frac{\mathrm{d}(\eta f_l)}{\mathrm{d}\eta} = 3V\frac{\mathrm{d}}{\mathrm{d}\eta}\left[f_l\frac{\mathrm{d}}{\mathrm{d}\eta}(f_u + Rf_l)\right]. \tag{3.5}$$

There are three key parameters that control the structure of the current: the volume ratio, F (2.11), the viscosity ratio V and the buoyancy ratio R (2.7). As these different parameters vary, one or other of the currents may detach from the source, and one of the currents may extend ahead of the other. We first examine a special family of solutions for which the ratio of the current depths is everywhere a constant. We then examine how the solutions change as the parameters R and V evolve away from these particular conditions. Since all solutions in this section are analytic, the algebra becomes quite involved in places. In order to assist the reader, it may be useful to refer to figure 2. The discussion (§ 3.1) commences with the special case in which the ratio of layer depths is constant (figure 2*d*). We then examine the evolution through the regimes shown in figures 2(*e*), (*f*) and (*g*) in which the lower layer is of relatively low viscosity or high density and runs ahead of the upper layer (§ 3.3). The discussion then returns to figure 2(*d*) and examines the evolution through the regimes shown in figures 2(*c*), (*b*) and (*a*) in which the upper layer is relatively less viscous and runs ahead of the lower layer (§ 3.4). Finally, a distinct limiting case in which both fluids have the same density, but different viscosity, is considered in § 3.5.

3.1. *Currents with constant layer depth ratio, $RV > 1 > V$; $F = F^* = (1-V)/(RV-1)$*

As a useful starting point, we first examine a special solution of the equations, which arises when the ratio of the current depths is a constant,

$$f_l = \alpha f_u. \tag{3.6}$$

Direct substitution into the global conservation of mass (2.10) identifies that $\alpha = F$, while substitution into the governing equations (3.4) and (3.5) then requires that

$$F = F^* = \frac{1-V}{RV-1}. \tag{3.7}$$

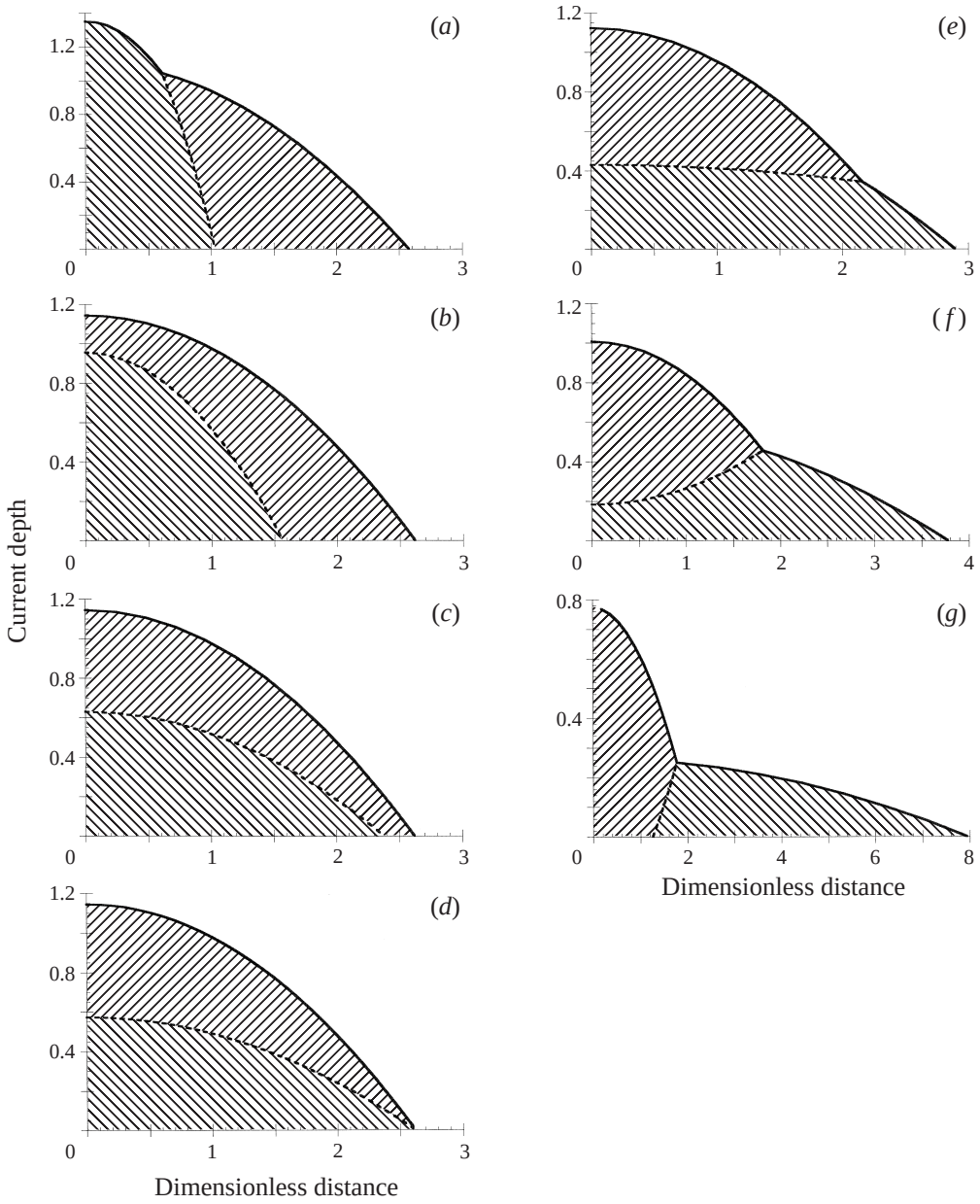

FIGURE 2. Example calculations for the shape of a two-layer current produced by a finite release of fluid, illustrating the transitions in current morphology as a function of the viscosity ratio of the two layers. In the calculations shown, the buoyancy ratio of the two layers is $R = 2$, the volume ratio $F = 1$, and the viscosity ratio V has values (*a*) 0.1 (upper layer ahead, $F < F_u$); (*b*) 0.3 (upper layer ahead, $RV < 1$, $F > F_u$); (*c*) 0.6 (upper layer ahead, $RV > 1 > V$, $F > F_u$); (*d*) 0.66 ($F = F^*$); (*e*) 0.9 (lower layer ahead, $RV > 1 > V$, $F > F_d$); (*f*) 2 (lower layer ahead, $V > 1$, $F > F_d$); (*g*) 20 (lower layer ahead, $F < F_d$).

Since $R > 1$, we deduce that $F^* > 0$ and so this solution is possible only if $RV > 1 > V$. This solution has the same form as the classical single-layer solution (3.1), so that (figure 2*d*)

$$f_u = \frac{1}{6(1+F)}(\eta_o^2 - \eta^2) \tag{3.8}$$

and

$$f_l = \frac{F}{6(1+F)}(\eta_o^2 - \eta^2), \tag{3.9}$$

with $\eta_o = (9(1+F))^{1/3}$. It follows that for this special solution, at all distances from the source, the speed has the same value in each layer.

3.2. *Currents with non-constant depth ratio*

If $F > F^*$, then the lower current is of relatively greater volume than that for which the noses of the upper and lower layers advance at the same rate for the given viscosity and buoyancy ratios. Thus we would expect it to advance ahead of the upper layer (figure 2*e*). Conversely, if $F < F^*$, then we might expect the leading edge of the lower layer to trail behind that of the upper layer (figure 2*c*). We now consider each of these cases in turn and extend the analysis to include the cases in which $V > 1$ or $RV < 1$.

By continuity from the case $F = F^*$ (§ 3.1), we anticipate that there is a parameter regime for which both layers are of finite depth at the origin. In this case, we set $f_l'(0) = f_u'(0) = 0$ and integrate (3.4) and (3.5) twice to obtain the relations

$$f_l + f_u = \tfrac{1}{6}(\eta_l^2 - \eta^2) \tag{3.10}$$

and

$$Rf_l + f_u = \frac{1}{6V}(\eta_u^2 - \eta^2), \tag{3.11}$$

where η_u and η_l are constants of integration. These equations are valid until either $f_u = 0$ or $f_l = 0$. Since the lower layer is denser than the upper layer, $R > 1$, we may then solve (3.10), (3.11) to obtain the expressions

$$f_l = \frac{\eta_u^2 - V\eta_l^2}{6V(R-1)} + \frac{(V-1)\eta^2}{6V(R-1)}, \tag{3.12}$$

$$f_u = \frac{RV\eta_l^2 - \eta_u^2}{6V(R-1)} + \frac{(1-RV)\eta^2}{6V(R-1)}. \tag{3.13}$$

In order that $f_u(0) > 0$ and $f_l(0) > 0$, we require $RV\eta_l^2 > \eta_u^2 > V\eta_l^2$.

Beyond the point $\eta = \eta^*$, at which the depth of one of the layers, j say, falls to zero, $f_j(\eta^*) = 0$, the depth f_i of the continuing current satisfies the equation (cf. 2.15)

$$\frac{\mathrm{d}\eta f_i}{\mathrm{d}\eta} = 3A_i \frac{\mathrm{d}}{\mathrm{d}\eta}\left(f_i \frac{\mathrm{d}f_i}{\mathrm{d}\eta}\right). \tag{3.14}$$

Here the value of the constant A_i depends on which layer extends the furthest, $A_l = RV$ and $A_u = 1$. This equation has first integral

$$f\frac{\mathrm{d}f}{\mathrm{d}\eta} = \frac{1}{3A_i}\eta f + B, \tag{3.15}$$

where B is a constant. By combining (3.12) and (3.13) with (3.15), one may show that

in order to satisfy the matching conditions for the depth and flux in the continuing current at $\eta = \eta^*$, (2.14), $B = 0$. Now (3.15) reduces to the simpler form

$$f = \frac{1}{6A_i}(\eta_e^2 - \eta^2), \tag{3.16}$$

where η_e is the dimensionless length of the current. Continuity of the depth of the continuing current at $\eta = \eta^*$ requires

$$\eta_e = \eta_u \quad \text{if} \quad i = l \quad \text{or} \quad \eta_e = \eta_l \quad \text{if} \quad i = u. \tag{3.17}$$

Finally, in order to determine the constants η_l and η_u, we apply the global conservation of mass in each layer (2.10),

$$\int_0^{\eta^*} f_j \, \mathrm{d}\eta = F_j \quad \text{and} \quad \int_0^{\eta_e} f_i \, \mathrm{d}\eta = F_i, \tag{3.18}$$

where $F_l = F$ and $F_u = 1$.

We now use this form of solution (equations (3.12), (3.13), (3.16)) to consider, in turn, the cases in which the lower (§ 3.3) and the upper (§ 3.4) layers extend ahead of the other layer. In both cases, we illustrate how the form of the solution evolves away from the simple case of parallel currents, $F = F^*$ (§ 3.1).

3.3. *Lower layer advances ahead of upper layer*

3.3.1. *Both layers attached to the source; $RV > 1 > V$; $F > F^* \geqslant 0$*

In this case, we expect the lower-layer current to extend ahead of the upper layer (figure 2*e*). The condition $f_u(\eta^*) = 0$ then determines the extent of the upper-layer current

$$\eta^* = \left(\frac{RV\eta_l^2 - \eta_u^2}{RV - 1}\right)^{1/2}. \tag{3.19}$$

Conservation of mass in the upper layer (3.18) gives the relation

$$\eta_u^2 = RV\eta_l^2 - 9^{2/3}V^{2/3}(R-1)^{2/3}(RV-1)^{1/3}. \tag{3.20}$$

Applying the conservation of mass in the lower layer we then find that

$$\eta_l^2 = \frac{9^{2/3}}{RV^{1/3}}\left((R-1)^{2/3}(RV-1)^{1/3} + (FR+1)^{2/3}\right) \tag{3.21}$$

and so

$$\eta_u^2 = 9^{2/3}V^{2/3}(1+FR)^{2/3}. \tag{3.22}$$

In order that the lower layer outruns the upper layer, we require $f_l(\eta^*) > 0$. Combining (3.12) and (3.20)–(3.22), this condition may be expressed in terms of F as

$$F > F^* = \frac{1-V}{RV-1}. \tag{3.23}$$

Finally, we note that this solution is consistent with the assumption that the lower layer remains attached to the source, $f_l(0) > 0$, provided that $\eta_u^2 > V\eta_l^2$. By substitution, it follows that this is always the case for $V < 1$ (see § 3.3.2).

These solutions are readily extended to describe the limiting case $V = 1$. In this special case, (3.12) reveals that the lower layer has constant depth in the region $0 < \eta < \eta^*$ in which the upper-layer depth falls to zero (3.6). We will return to this result in § 5 when considering the motion of continuously stratified currents.

3.3.2. *Lower layer less viscous but remains attached to the source, $V > 1$; $F > F_d$*

When the viscosity of the upper layer exceeds that of the lower layer, $F^* < 0$ and the form of the solution changes. Now the depth of the lower-layer current initially increases with distance from the origin ((3.12); figure 2*f*), while the depth of the upper layer decreases to zero. Further from the source, the lower-layer depth falls to zero. However, as long as the current remains attached to the source, the solutions (3.12) and (3.13), subject to the constraints (3.21) and (3.22), still apply (e.g. figure 2*f*). These solutions may be used to determine the limiting case in which $f_l(0) = 0$ and hence $\eta_u = V\eta_l$. This limiting case corresponds to the condition

$$F = F_d = \frac{1}{R}\left(\left(\frac{RV-1}{R-1}\right)^{1/2} - 1\right) \tag{3.24}$$

and for $F > F_d$ the lower-layer current remains attached to the source (figure 3 below). For smaller volumes of fluid, the lower, dense and less-viscous layer will in fact detach from the source (figure 2*g*), as described below (§ 3.3.3). Note that, as mentioned in § 3.3.1, in the case for which $V < 1$, $F_d < 0$ and so both layers are always attached to the source.

3.3.3. *Lower layer detaches from the source, $V > 1$, $F < F_d$*

If the volume of the less-viscous lower layer is sufficiently small, for the given viscosity and buoyancy ratios, $F < F_d$, then all the lower-layer fluid may detach from the source. In this case, there are three distinct regions in the flow (figure 2*g*). Near the origin, the current is entirely composed of upper-layer fluid, $0 < \eta < \eta^+$. There is an intermediate region in which both layers of fluid are present, $\eta^+ < \eta < \eta^*$, and finally, the lower-layer fluid forms the leading edge of the current, $\eta^* < \eta < \eta_e$. In the region in which both fluids are present, the solution has the same form as given by equations (3.12), (3.13). η^+ is the position at which the lower-layer depth (3.12) is zero,

$$\eta^{+2} = \frac{V\eta_l^2 - \eta_u^2}{V-1} \tag{3.25}$$

and η_e is the maximum extent of the current. The maximal extent of the upper layer is given by (3.13)

$$\eta < \eta^* = \left(\frac{RV\eta_l^2 - \eta_u^2}{RV-1}\right)^{1/2}. \tag{3.26}$$

The condition that the two currents overlap, $\eta^+ < \eta^*$, requires that $V\eta_l^2 > \eta_u^2 > \eta_l^2$.

The continuity of depth and speed of each layer at the points $\eta = \eta^+$ and $\eta = \eta^*$, which bound the region in which both fluid layers are present, provide useful constraints on the flow solutions. Near the origin, $\eta < \eta^+$, the upper layer is described by a solution of the form (cf. (3.16))

$$f_u = \tfrac{1}{6}(\eta_s^2 - \eta^2). \tag{3.27}$$

Coupling this with the matching conditions at $\eta = \eta^+$ where the depth of the lower layer is first non-zero (3.25) gives the result

$$\eta_s = \eta_l. \tag{3.28}$$

In the region $\eta > \eta^*$, ahead of the upper layer, the lower layer is described by a

solution of the form (cf. (3.16))

$$f_l = \frac{1}{6RV}(\eta_e^2 - \eta^2). \tag{3.29}$$

The matching conditions at $\eta = \eta^*$ (2.14) give the result

$$\eta_e = \eta_u. \tag{3.30}$$

Using these solutions, we may now apply the global conservation of mass in both the upper and lower layers. This leads to two nonlinear equations for η_u and η_l,

$$\frac{RV-1}{V(R-1)}\left(\frac{RV\eta_l^2 - \eta_u^2}{RV-1}\right)^{3/2} - \frac{V-1}{V(R-1)}\left(\frac{V\eta_l^2 - \eta_u^2}{V-1}\right)^{3/2} = 9 \tag{3.31}$$

and

$$\frac{1}{RV}\eta_u^3 + \frac{V-1}{V(R-1)}\left(\frac{V\eta_l^2 - \eta_u^2}{V-1}\right)^{3/2} - \frac{RV-1}{RV(R-1)}\left(\frac{RV\eta_l^2 - \eta_u^2}{RV-1}\right)^{3/2} = 9F. \tag{3.32}$$

Numerical solution of these equations determines the full solution for both the upper- and lower-layer currents (e.g. figure 2*g*).

In the limit $V \to \infty$, we expect the lower layer to run ahead of the upper layer, and each layer should behave essentially as a single layer. From the above algebraic relations (3.31), (3.32) we see that in this limit, the extent of the lower layer $\eta_u \to (9RFV)^{1/3}$, as for the classical single-layer solution (3.1). Furthermore, we find that $\eta_l \to 9^{1/3}$ and so the extent of the upper layer $\eta^* \to 9^{1/3}$, again as in the classical single-layer flow (3.1). We also note that the extent of the intermediate region, in which both layers are present, becomes vanishingly thin. In § 3.5 we examine a different limit, $R \to 1$, in which this intermediate region again becomes vanishingly thin.

3.4. *Upper layer advances ahead of lower layer*

3.4.1. *Both layers attached to the source, $F < F^* \leqslant \infty$*

If $F < F^*$, we expect the upper layer to extend beyond the lower layer (figure 2*c*). Equation (3.12) together with the condition $f_l(\eta^*) = 0$ determines that

$$\eta^* = \left(\frac{\eta_u^2 - V\eta_l^2}{1-V}\right)^{1/2}. \tag{3.33}$$

Using the solution (3.12), it follows that the conservation of mass in the lower layer (3.18) requires

$$\eta_u^2 = V\eta_l^2 + 9^{2/3}V^{2/3}F^{2/3}(R-1)^{2/3}(1-V)^{1/3}. \tag{3.34}$$

In the region ahead of the lower-layer current, $\eta > \eta^*$, the upper-layer current has shape (3.16)

$$f_u = \tfrac{1}{6}(\eta_e^2 - \eta^2). \tag{3.35}$$

Applying conservation of mass in the upper layer together with the matching condition (3.17) at the front of the lower layer, $\eta = \eta^*$, identifies that

$$\eta_l^2 = 9^{2/3}(F+1)^{2/3}. \tag{3.36}$$

In order that the upper layer outruns the lower layer, we require $f_u(\eta^*) > 0$. By combining this with (3.13) and (3.34), (3.36), it follows that this condition is equivalent to $F < F^*$.

Finally, the condition that the upper layer remains attached to the source, $f_u(0) > 0$, requires that $\eta_u^2 > RV\eta_l^2$. By substitution, we find that this condition is always the case for $RV > 1$ (§ 3.4.2).

In the limiting case in which $RV = 1$ and $F^* \to \infty$, the solutions still apply, but now the upper layer has a fixed depth until the point at which the depth of the lower layer falls to zero (3.12).

3.4.2. *Upper layer attached to the source; $RV < 1$, $F < F_u$*

As the upper layer becomes less viscous, it tends to run further ahead of the more-viscous lower layer and the form of the solution changes (figure 2*b*). If the upper layer is sufficiently large compared to the lower layer it remains attached to the origin. However, now the depth of the upper layer increases with distance from the origin in the region $0 < \eta < \eta^*$, as the depth of the lower layer falls to zero (figure 2*b*). Beyond this region, $\eta^* < \eta < \eta_e$, the upper-layer depth then falls to zero. The solutions (3.12), (3.13) apply near the source, in the region $0 < \eta < \eta^*$. In order that the upper layer remains attached to the source we require $RV\eta_l^2 > \eta_u^2$. Using (3.34), (3.36), it follows that this requires (figure 3)

$$F < F_u = \frac{1}{\big((1-V)/[V(R-1)]\big)^{1/2} - 1}. \tag{3.37}$$

Note that as $RV \to 1$, $F_u \to \infty$ and so, as mentioned in § 3.4.1, for $RV > 1$, the upper layer remains attached to the source.

3.4.3. *Upper layer detaches from the source: $F > F_u$; $F^* < 0$*

For $F > F_u$, the upper layer detaches from the source, running ahead of the more-viscous lower layer (figure 2*a*). As in § 3.3.3, there are three distinct regions of the current: in this case, there is region near the source containing only lower-layer fluid, $0 < \eta < \eta^+$, a region containing both layers, $\eta^+ < \eta < \eta^*$, and a region containing only upper-layer fluid, $\eta^* < \eta < \eta_e$. As in § 3.3.3, the intermediate region, containing both layers of fluid is described by (3.12) and (3.13). The upper layer lies in the region $\eta^+ < \eta < \eta^e$ while the lower layer lies in the region $0 < \eta < \eta^*$. In order that there is an overlap between the two layers, $\eta^+ < \eta^*$, we require $RV\eta_l^2 > \eta_u^2 > \eta_l^2$. The solutions in the regions containing a single layer of fluid are analogous to (3.27) and (3.29), but now have the form $f_u = (\eta_e^2 - \eta^2)/6$ and $f_l = (\eta_s^2 - \eta^2)/(6RV)$ since the upper layer advances ahead of the lower layer. As in § 3.3.3, the solution is found by matching these solutions for a single layer of fluid with the solutions (3.12), (3.13) for the intermediate region in which both fluids are present. Now we find that $\eta_e = \eta_l$ and $\eta_s = \eta_u$.

The system is completed with the equations for global conservation of mass in each layer. Combining these constraints, we derive the two nonlinear equations relating η_u and η_l (cf. (3.31), (3.32))

$$\frac{1-RV}{V(R-1)}\left(\frac{\eta_u^2 - RV\eta_l^2}{1-RV}\right)^{3/2} - \frac{1-V}{V(R-1)}\left(\frac{\eta_u^2 - V\eta_l^2}{1-V}\right)^{3/2} + \eta_l^3 = 9 \tag{3.38}$$

and

$$\frac{1-V}{V(R-1)}\left(\frac{\eta_u^2 - V\eta_l^2}{1-V}\right)^{3/2} - \frac{1-RV}{RV(R-1)}\left(\frac{\eta_u^2 - RV\eta_l^2}{1-RV}\right)^{3/2} = 9F. \tag{3.39}$$

Solution of these algebraic equations then determines the exact similarity solution (e.g. figure 2*a*).

It is interesting to note that in the limit $V \to 0$, the two layers become essentially decoupled. The upper layer runs ahead of the lower layer, and its length $\eta_l \to 9^{1/3}$ as in the classical single-layer solution (3.1). We also find that $\eta_u \to (9FRV)^{1/3}$ so that the length of the lower layer has asymptotic value $\eta^* \to (9RFV)^{1/3}$. Since we have defined dimensionless properties relative to the top layer, then again we see that this limit corresponds to the classical solution for a single-layer current (3.1). Finally, as in § 3.3.3, we note that in this limit the intermediate zone, in which both layers are present, becomes vanishingly thin.

3.5. *Equal density but different viscosity,* $R = 1, V \neq 1$

One limiting case is that in which the two fluids have the same density, $R = 1$, but different viscosity. Now, solutions (3.12) and (3.13) break down. However, by considering the limit $R \to 1$, we see that in fact the interface between the two layers becomes vertical, with the less-viscous fluid advancing ahead of the more-viscous layer. For example, if we consider the case $V < 1$, the lower layer is more viscous and trails the upper layer. The variation of depth as a function of distance from the source then has the form

$$f_l = \frac{1}{6V}(\eta_u^2 - \eta^2) \quad \text{for} \quad 0 < \eta < \eta^* \tag{3.40}$$

and

$$f_u = \tfrac{1}{6}(\eta_l^2 - \eta^2) \quad \text{for} \quad \eta^* < \eta < \eta_l. \tag{3.41}$$

Continuity of the current depth at $\eta = \eta^*$ is given by $f_l(\eta^*) = f_u(\eta^*)$ and yields the algebraic relation

$$\eta^{*2} = \frac{V\eta_l^2 - \eta_u^2}{V - 1}. \tag{3.42}$$

The global conservation of mass in each layer leads to the additional relations

$$(3\eta_u^2 - \eta^{*2})\eta^* = 18VF \tag{3.43}$$

and

$$2\eta_l^3 - 3\eta_l^2\eta^* + \eta^{*3} = 18. \tag{3.44}$$

Solution of (3.42)–(3.44) gives solutions for η_u, η^* and η_l in terms of F and V. The results illustrate how the relative extent of the two layers is strongly controlled by the viscosity contrast.

3.6. *Summary of regimes*

The different flow regimes which develop as F and V change, for a given value of R, may be summarized in a simple regime diagram (figure 3). The physical origin of the transitions between the different flow regimes may also be understood from this diagram. First we note that equation (3.7), $F = F^*$, may be re-written in terms of a critical viscosity ratio

$$V = V^* = \frac{1 + F}{1 + RF}. \tag{3.45}$$

As seen from figure 3, if $V > V^*$, then the lower layer advances ahead of the upper layer, while for $V < V^*$, the upper layer advances ahead of the lower layer. Since V^* always lies in the interval $0 < V^* < 1$, it is therefore instructive to examine how, for a given value of the volume and buoyancy ratios of the layers, the flow configuration evolves with viscosity ratio. For high viscosity ratio, with the upper layer being more

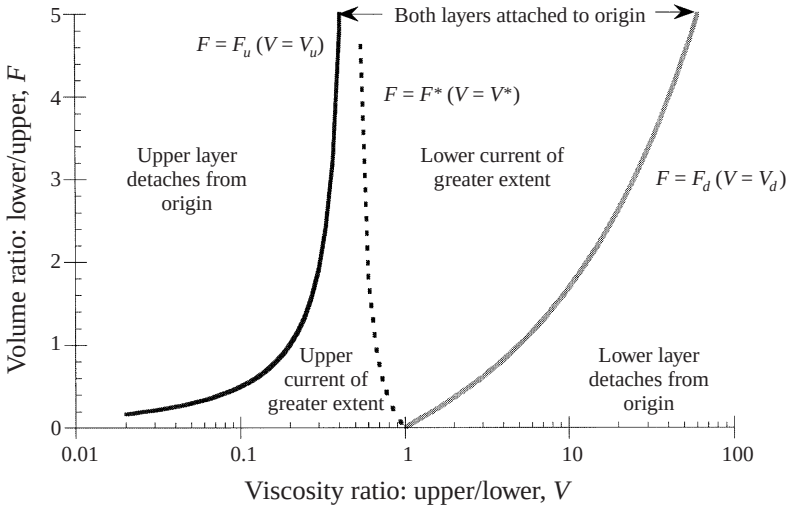

FIGURE 3. Regime diagram illustrating how the different flow morphologies depend on the viscosity ratio V and volume ratio F of the two fluid layers. Curves are given for a density ratio $R = 2$.

viscous, $V \gg 1$, the lower layer runs ahead of the upper layer, detaching from the origin (figure 2*g*). As the viscosity ratio decreases, the trailing edge of the lower layer moves back towards the origin and eventually makes contact with the origin (figure 2*f*). This occurs when $F = F_d$ (3.24); this condition may be re-expressed in terms of V as

$$V = V_d = \frac{(RF + 1)^2(R - 1) + 1}{R}. \tag{3.46}$$

Thus for $V > V_d$ the lower layer is detached from the source. As the viscosity ratio continues to fall, the lower-layer speed begins to decrease towards that of the upper layer (figure 2*e*). Eventually, the current passes through the point $V = V^*$ ($F = F^*$) at which the ratio of the current depths is everywhere the same, and hence, at each point, the speed of each layer is the same (figure 2*d*). As the viscosity ratio decreases further, the upper layer begins to flow more rapidly than the lower layer, and hence overruns the lower layer (figure 2*c*). For even smaller viscosity ratios, the upper layer eventually detaches from the source (figure 2*a*, *b*). This first occurs when $F = F_u$ (3.37). This condition may be re-expressed in terms of V as

$$V = V_u = (1 + (R - 1)(1/F + 1)^2)^{-1}. \tag{3.47}$$

Thus, for $V < V_u$, the upper layer is detached from the source.

As the buoyancy ratio of the layers changes, the boundaries between these different transition points also evolves, although the general evolution through the different regimes remains the same. For example, in figure 4, we present the regime diagram for the case $R = 1.1$. Now, the critical viscosity ratios at which either the upper or the lower layer separates from the source are both closer to the point $V = 1$ (cf. figure 3). In the case $R = 1$, we showed in § 3.5 that the interface between the two fluid layers is vertical. For a given buoyancy ratio $R > 1$, the vertical interface between the fluids becomes distorted, and the degree of distortion increases as either R increases, or $|V - 1|$, the dimensionless difference in viscosity, decreases. As a result, the critical value of V at which the interface becomes distorted sufficiently to intersect the origin is closer to $V = 1$ for smaller R.

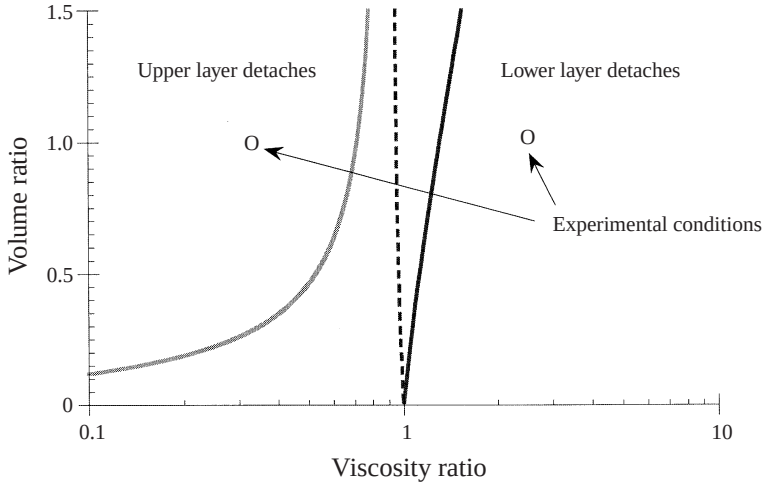

FIGURE 4. Regime diagram illustrating how the different flow morphologies depend on the viscosity ratio V and volume ratio F of the two fluid layers. Curves are given for the density ratio $R = 1.1$ corresponding to the fluids used in the laboratory experiments. The two circles indicate the properties of the two experiments described in sections 4.1 and 4.2.

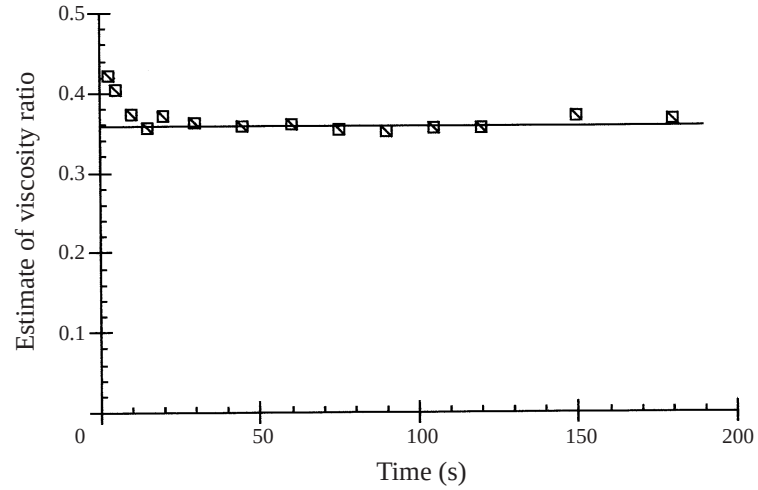

FIGURE 5. Variation of the viscosity ratio as a function of time as determined from the two control experiments (§4.1). In the long time limit, $V \to 0.36$.

As a final comment on these solutions, equation (3.45) has the interesting limits $V^* = 1$ as $F \to 0$ and $V^* = 1/R$ as $F \to \infty$. This means that in order to effectively displace a dense fluid with a less-dense fluid, the viscosity of the less-dense fluid should be greater than that of the underlying dense fluid irrespective of the volume of less-dense fluid added to the system. Otherwise the low-density fluid will simply run off the dense layer and spread ahead. Similarly, in order to displace a low-density fluid with a more-dense fluid, the denser fluid should have viscosity greater than that of the upper layer times the buoyancy ratio of the two layers, irrespective of the volume of dense fluid added to the system. Otherwise it will spread under and ahead of the less-dense layer.

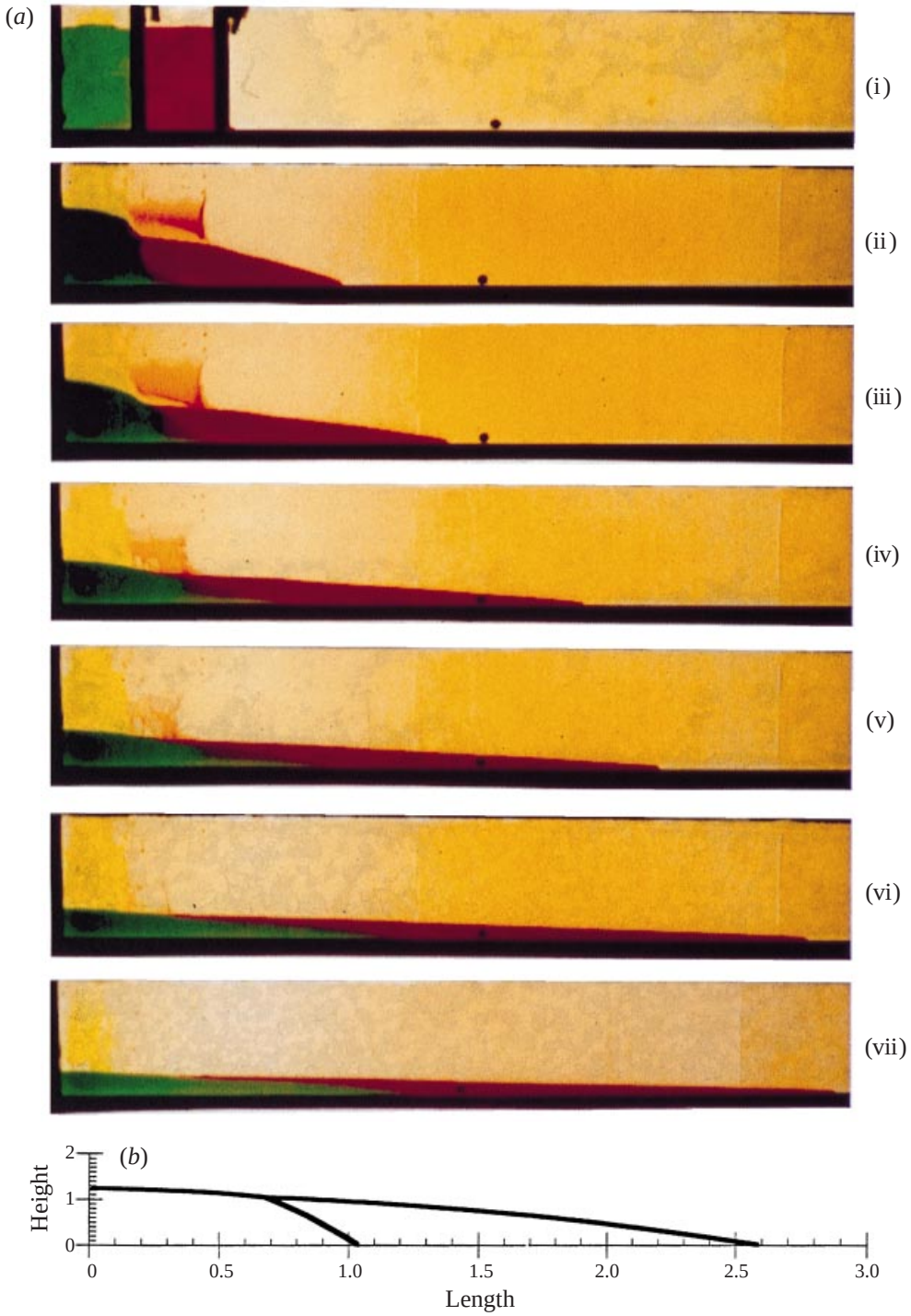

FIGURE 6. (*a*) Sequence of photographs for experiment 4.1, for which $R = 1.1$, $V = 0.36$. The photographs show the evolution of the current towards the self-similar shape. Photographs were taken at the times (i) 0, (ii) 14, (iii) 51, (iv) 131, (v) 189, (vi) 399 and (vii) 675 s. The glycerol is dyed red and the syrup is dyed green. (*b*). Prediction of the current shape from the theory of § 3 for comparison with the experiments.

4. Experimental investigation

We have conducted a series of laboratory experiments to examine the propagation of two-layer gravity currents in a Hele-Shaw cell for comparison with the model described above. The cell consisted of two Perspex walls, of height 150 mm and length 1000 mm, separated by a gap of width $b = 3$ mm. For the present experiments, the flow in the cell had Reynolds number of order 0.01–0.1, and so provides a good analogue for flow in a porous layer (Bear 1972). Indeed, the flow is governed by the model of § 2, with a permeability of value $b^2/12$, provided that the current remains deeper than the width of the cell so that the frictional stresses with the floor of the cell and between the layers may be neglected.

In the experiments, the two layers of fluid were placed side by side in two locks at the end of the cell, with the more-viscous fluid closer to the end (see figure 6*a*i below). The two lock gates were then removed and the ensuing evolution of the flow was recorded by video and photograph. For convenience, the two fluids used were golden syrup (lower layer) and glycerol (upper layer), each diluted with a small quantity of water to vary the viscosity. The dilution was small, and in all the experiments the density contrast $R = 1.1 \pm 0.05$. The viscosity ratio of the two fluid mixtures, V, was determined by conducting two control experiments in which the location of the nose of a single-layer gravity current of a specific volume of each fluid was measured at a predetermined set of times, t_i (cf. Huppert & Woods 1995). This produced two sets of data, $x_1(t_i)$ and $x_2(t_i)$. By comparison with the similarity solution (3.1), it follows that when each of the currents has adjusted to self-similar form, the viscosity ratio is given by $\mu_1/\mu_2 = (\rho_1/\rho_2)(x_2(t)/x_1(t))^3$.

In figure 4, we show the regime diagram for the case $R = 1.1$. For such a small density contrast, we see that the less-viscous layer typically separates from the source, unless the viscosities are very similar. By varying the dilution, we were therefore able to examine situations in which either the upper or the lower layer was more viscous and is predicted to separate from the source. We now describe two experiments, corresponding to the experimental conditions shown on figure 4.

4.1. *Upper layer less viscous*

In this experiment, the viscosity ratio had value $V \sim 0.36$ (figure 5), so that from figure 4 we expect the upper layer to separate from the source and run ahead of the lower layer. In figure 6(*a*) we present a series of photographs which illustrate the time evolution of the current. The viscous syrup (green) was placed in the outer lock, and the glycerol (red) in the inner lock. After a rapid initial slump, the current acquires the two-layer structure anticipated by the model of § 3, with the glycerol advancing ahead of the syrup. Note that during the initial slump (figure 6*a*ii; 14 s), the no-slip condition on the walls of the cell causes the interface between the two layers of fluid to become distorted; the viscous syrup flows into the central part of the cell, while the walls of the cell remain covered with glycerol. However, as the flow spreads and the speed decreases, the buoyancy contrast between the layers restores the interface to a well-defined front, as assumed in the model (figure 6*a*iv–vii). Figure 7 shows that the leading edge of each layer of the current increases as $t^{1/3}$, in good accord with the prediction that the current evolves in a self-similar fashion following release (§ 3.4.3). The observed shape of the current is also in good accord with the model prediction (cf. figures 6*a* and 6*b*), with the prediction of the maximal extent of the lower layer being within about 10–20% of the observations. The region of overlap of the two layers predicted by the model is somewhat shorter than that observed in the experiments; in part, this may be a result of the viscous stresses between the lower

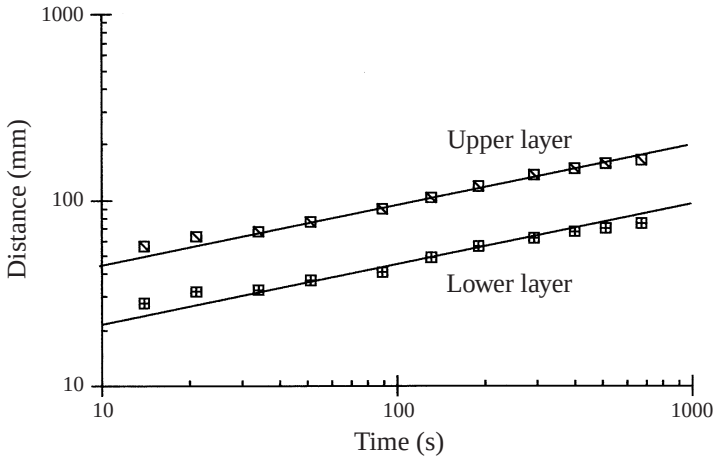

FIGURE 7. Variation of the extent of the upper and lower layers with time for experiment, § 4.1. The solid lines have slope 1/3.

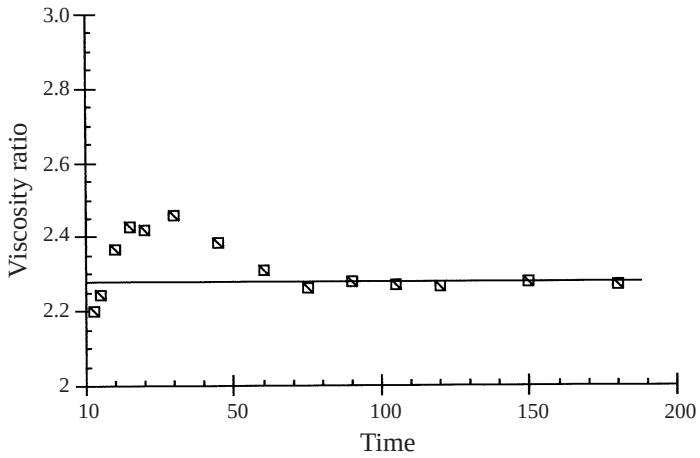

FIGURE 8. Variation of the viscosity ratio as a function of time as determined from the two control experiments (§ 4.2). In the long-time limit, $V \rightarrow 2.27$.

layer and the floor of the cell and between the upper and lower layers. These stresses become dominant as the relevant layer thickness decreases to values similar to the width b of the cell. In comparison to the idealized model predictions, which only account for the frictional stresses with the vertical walls of the cell, in the experiments these additional stresses act to increase the region of overlap between the two fluids.

4.2. *Lower layer less viscous*

In this second experiment, we determined that the viscosity ratio between the upper and lower layers, $V \sim 2.27$ (figure 8), so that from figure 4 we expect the lower layer to separate from the source and run ahead of the lower layer. Figure 9(*b*) shows a sequence of photographs illustrating the evolution of the current after the lock gates were removed. Here, the dilute yellow syrup layer is denser but less viscous than the blue glycerol layer. As expected, the dilute syrup runs ahead of the glycerol and the current again acquires a shape similar to that predicted by the model (figure 9*b*).

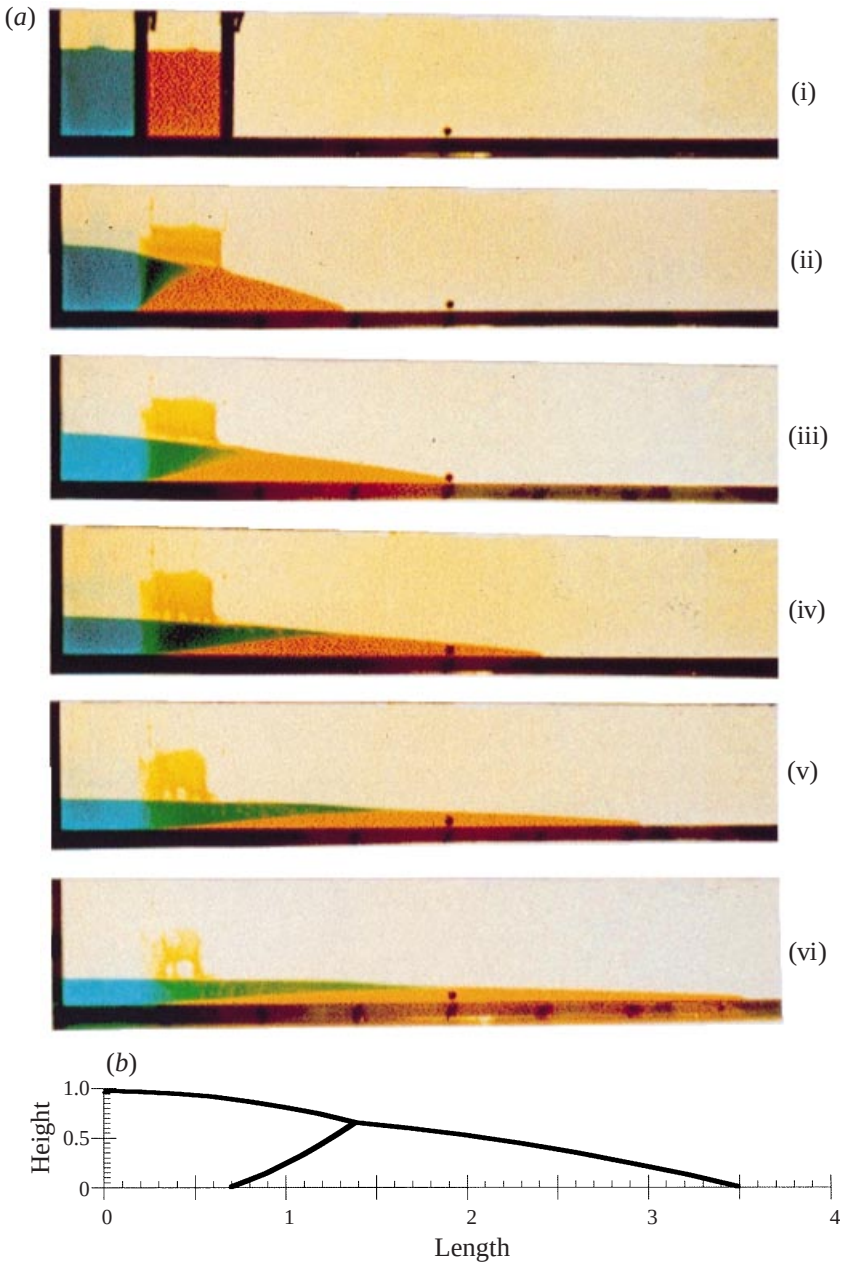

FIGURE 9. (*a*) Sequence of photographs for experiment in § 4.2 for which $R = 1.1$, $V = 2.2$. The photographs show the evolution of the current towards the self-similar shape. Photographs were taken at the times (i) 0, (ii) 7, (iii) 29, (iv) 63, (v) 128, and (vi) 246 s. The glycerol is dyed blue and the syrup is dyed yellow. (*b*) Prediction of the current shape from the theory of § 3 for comparison with the experiments.

Analysis of the time evolution of the current confirms that to good approximation, the maximal extent of both the upper and lower layers increases with $t^{1/3}$ (figure 10), again supporting the prediction that the current evolves in a self-similar fashion (§ 3.3.3). Again, although the predicted shape of the current is in reasonable accord

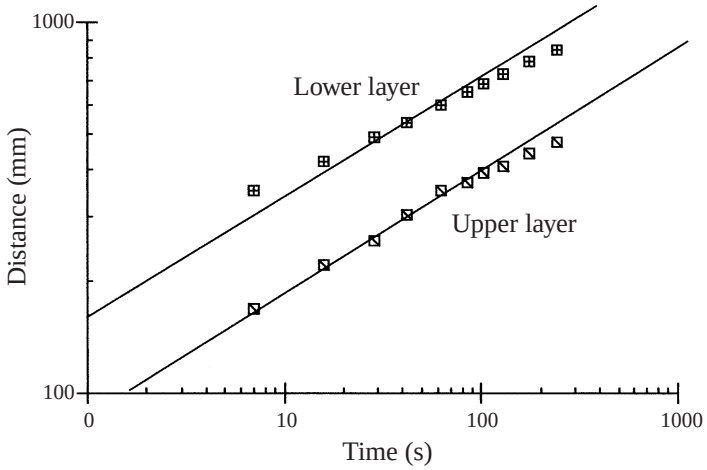

FIGURE 10. Variation of the extent of the upper and lower layers with time for experiment in § 4.2. The solid lines have slope 1/3.

FIGURE 11. Long-time structure of a current produced from a source in which the low-viscosity upper layer was initially placed above the lower layer. In comparison with the flow shown in figure 6, there is a narrow strip of upper layer fluid which extends back to the source. This is a result of the viscous stress with the underlying layer.

with the model (figure 9), the viscous stresses between the two layers and between the lower layer and the cell floor appear to stretch out the zone of overlap of the two layers by 20–30% in comparison with the idealized model prediction. There is a slow drift of the experiments away from the self-similar solution at long times. This may be the result of the friction with the lower boundary as described by Huppert & Woods (1995).

4.3. *Other regimes and effect of initial conditions*

The above experimental observations provide very good evidence that after some initial transient, the flow is approximately described by the self-similar solutions described in § 3. This initial transient will depend on the initial configuration of the two fluids, and more complex transient flow patterns may develop with more irregular source conditions. For example, figure 11 shows the long-time profile of an experiment in which initially the low-viscosity upper layer was located vertically above the dense lower layer at the source. Although there was some intermingling of the fluid layers during the initial stages of the process, as the upper layer slumps ahead of the lower layer, the current does eventually segregate into two well-defined layers. As predicted by the model (cf. § 4.1), the main volume of the red upper layer lies some distance ahead of the source. However, one effect of the viscous stress between the two layers of fluid is the appearance of a thin strip of red upper-layer fluid which extends all way back to the source above the lower layer.

5. Continuous release of fluid

With a continuous release of fluid, both layers always remain attached to the origin. Again, it is of interest to determine which layer extends further from the source. For a continuous release of fluid, the model equations (2.4)–(2.6) admit solutions of the form

$$h_l(x,t) = H(\Omega t)^{1/3} f_l(\eta), \tag{5.1}$$

$$h_u(x,t) = H(\Omega t)^{1/3} f_u(\eta), \tag{5.2}$$

where $\eta = x/H(\Omega t)^{2/3}$, $H = Q_u/S\phi$ and $\Omega = S^2\phi/Q_u$, with $\phi\int_0^{L_l} h_l\,\mathrm{d}x = FQ_ut$, and $\phi\int_0^{L_u} h_u\,\mathrm{d}x = Q_ut$ being the volume of each current after a time t.

We deduce that f_l and f_u satisfy the equations

$$f_l - 2\eta\frac{\mathrm{d}f_l}{\mathrm{d}\eta} = 3V\frac{\mathrm{d}}{\mathrm{d}\eta}\left(f_l\left(R\frac{\mathrm{d}f_l}{\mathrm{d}\eta} + \frac{\mathrm{d}f_u}{\mathrm{d}\eta}\right)\right) \tag{5.3}$$

while

$$f_u - 2\eta\frac{\mathrm{d}f_u}{\mathrm{d}\eta} = 3\frac{\mathrm{d}}{\mathrm{d}\eta}\left(f_u\left(\frac{\mathrm{d}f_l}{\mathrm{d}\eta} + \frac{\mathrm{d}f_u}{\mathrm{d}\eta}\right)\right), \tag{5.4}$$

with

$$\int_0^{\lambda_l} f_l\,\mathrm{d}\eta = F \quad \text{and} \quad \int_0^{\lambda_u} f_u\,\mathrm{d}\eta = 1, \tag{5.5}$$

where λ_l and λ_u are the dimensionless lengths of the upper- and lower-layer currents.

In the special case in which

$$f_l = Ff_u \tag{5.6}$$

throughout the length of the current, we find that both currents have the same horizontal extent. In order that equations (5.3) and (5.4) are satisfied, we then require that

$$F = F^* = \frac{1-V}{VR-1}. \tag{5.7}$$

This is the same condition as derived in § 3.1 for a finite release of fluid, and requires that $V < 1 < VR$. Again, if $F > F^*$, then we expect that the upper layer extends beyond the lower layer, and conversely in the case $F < F^*$. Therefore equation (5.7) provides the boundary between the two forms of solution. Unfortunately, the system of equations is not tractable analytically, and so the detailed form of the solutions in other cases can only be determined numerically. One key difference between these solutions and those of § 3 is that both currents remain attached to the source. However, as V increases above unity, so that F^* becomes negative, then we expect that most of the fluid in the low-viscosity lower layer will advance ahead of the upper layer. Similarly, as RV falls below unity, the upper layer becomes less viscous and most of the fluid in the upper layer is expected to lie ahead of the lower layer.

We have solved the system of equations numerically to determine the different flow regimes which develop as a function of the controlling parameters. In order to solve the equations, we require that the flux and depth of each layer is continuous at the point at which the depth of one or other of the currents falls to zero, and we consider in turn the cases in which the upper and the lower current is of greater extent.

5.1. *Upper layer of greater extent, $\eta_u > \eta_l$*

To proceed with the numerical solution, it is convenient to define the variable

$$\zeta = \eta/\eta_u \tag{5.8}$$

and

$$(n_l, n_u) = \eta_u^2 (f_u, f_l) \tag{5.9}$$

so that the upper layer lies in the region $0 < \zeta < 1$ and the lower layer in the region $0 < \zeta < \zeta_l = \eta_l/\eta_u$; n_l and n_u satisfy the equations (cf. (5.3), (5.4))

$$n_u - 2\zeta \frac{\mathrm{d}n_u}{\mathrm{d}\zeta} = 3\frac{\mathrm{d}}{\mathrm{d}\zeta}\left(n_u\left[\frac{\mathrm{d}n_u}{\mathrm{d}\zeta} + \frac{\mathrm{d}n_l}{\mathrm{d}\zeta}\right]\right), \tag{5.10}$$

$$n_l - 2\zeta \frac{\mathrm{d}n_l}{\mathrm{d}\zeta} = 3V\frac{\mathrm{d}}{\mathrm{d}\zeta}\left(n_l\left[R\frac{\mathrm{d}n_l}{\mathrm{d}\zeta} + \frac{\mathrm{d}n_u}{\mathrm{d}\zeta}\right]\right), \tag{5.11}$$

but the global mass conservation now has the form

$$\int_o^1 n_u \,\mathrm{d}\zeta = \eta_u^3 \quad \text{and} \quad \int_0^{\zeta_l} n_l \,\mathrm{d}\zeta = \eta_u^3 F. \tag{5.12}$$

Conservation of upper-layer flux at the point where the lower current terminates $\zeta = \zeta_l$ requires

$$\frac{\mathrm{d}n_u}{\mathrm{d}\zeta}(\zeta_l+) = \frac{\mathrm{d}n_u}{\mathrm{d}\zeta}(\zeta_l-) + \frac{\mathrm{d}n_l}{\mathrm{d}\zeta}(\zeta_l-), \tag{5.13}$$

while a power series solution for the depth of each current about $\zeta = \zeta_l$ (cf. Huppert 1986) shows that

$$\frac{\mathrm{d}n_l}{\mathrm{d}\zeta}(\zeta_l-) = \frac{1}{3VR}\left(-2\zeta_l - 3V\frac{\mathrm{d}n_u}{\mathrm{d}\zeta}(\zeta_l-)\right). \tag{5.14}$$

Finally, at the leading edge of the current, $\zeta = 1$, the upper-layer depth satisfies

$$\frac{\mathrm{d}n_u}{\mathrm{d}\zeta} = -\frac{2}{3}. \tag{5.15}$$

By numerically integrating the equations backwards from $\zeta = 1$, subject to these boundary conditions, we are able to find the shape of the two-layer currents and the value of F for each value of ζ_l. For each set of parameters (R, V), we search for the value of ζ_l, $0 < \zeta_l < 1$, such that F has the desired value. In all the figures presented below, the dimensionless solutions n_u, n_l are shown as functions of ζ.

Figure 12(*d–g*) illustrates the dependence of the structure of the current on the buoyancy ratio of the layers. In these calculations, the viscosity ratio of the upper to lower layers, $V = 0.1$, so that the upper-layer fluid is considerably less viscous than the lower layer while $F = 1$. For small values of the buoyancy ratio, $R = 1.01$ (figure 12*g*), the low-viscosity upper layer runs over and ahead of the lower layer. At its leading edge, the depth of the lower layer falls to zero rapidly. This is expected, by analogy with the finite release problem for which the case $R = 1$ (§ 3.3.1) showed that the interface between the two layers becomes vertical. As the lower layer becomes progressively more dense (figure 12(*e, f*)), the difference in viscosity is partially counterbalanced by the density, and an increasing fraction of the upper layer remains above the dense lower layer. Eventually, at the critical point, at which $F^* = F = 1$, which requires $R = 19$, (5.7), the depths of the upper and lower layers become identical at all points (figure 12(*d*)). As the parameters pass through the point $RV = 1$, corresponding to $F^* \to \infty$, an inflection is seen to develop in the depth of the current.

Figure 13(*d–g*) illustrates the change in structure of the current as the viscosity ratio evolves, for a fixed value of the buoyancy ratio, $R = 2$. For small values of the upper-layer viscosity (figure 13(*g*)) the upper layer runs ahead of the lower layer,

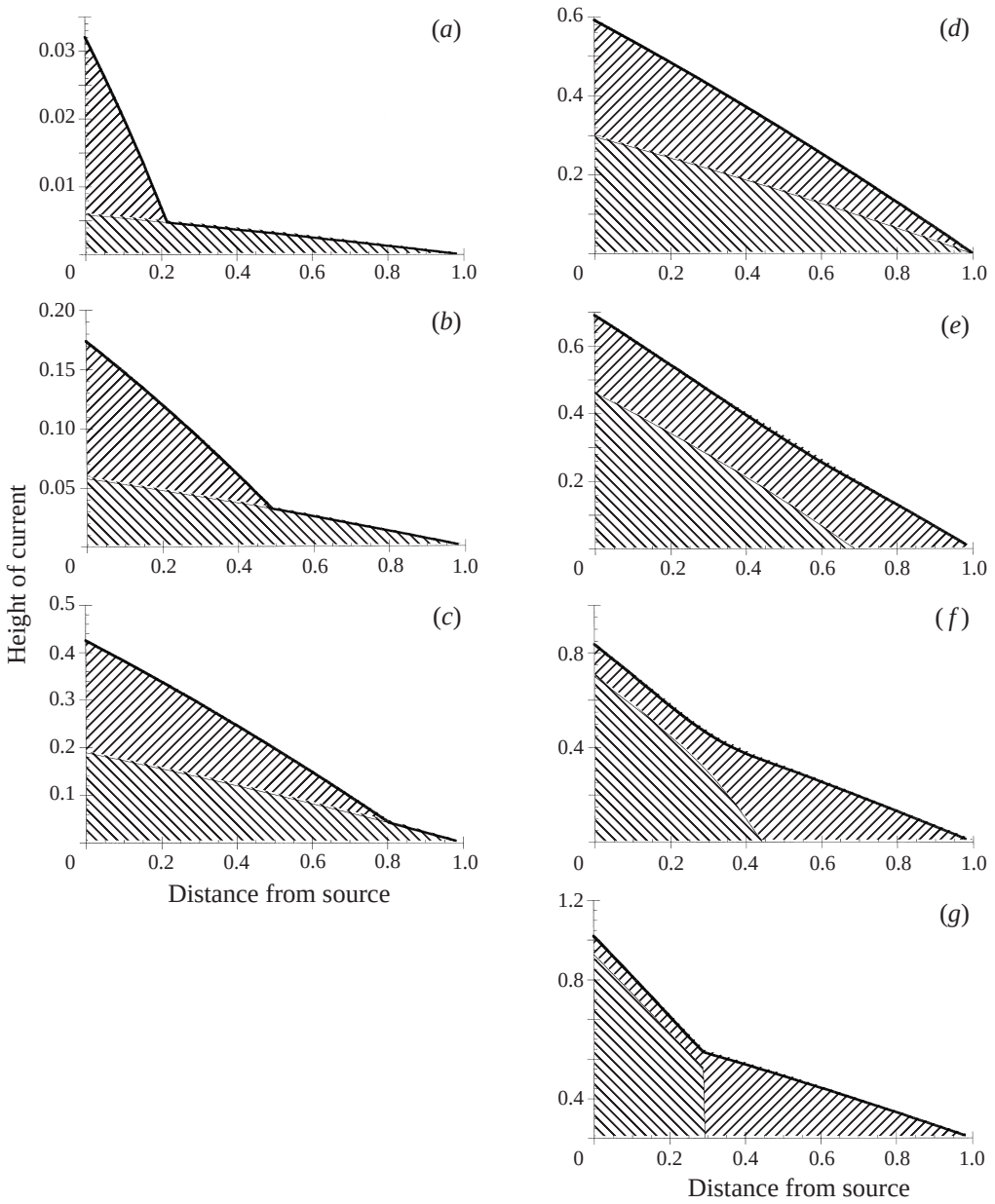

FIGURE 12. Variation of the flow morphology in a two-layer current produced by a maintained source of fluid as a function of the density ratio. In all calculations the flux ratio $F = 1$, while the viscosity ratio has value 0.1. The density ratio takes the values (*a*) $R = 1000$; (*b*) $R = 100$; (*c*) $R = 30$; (*d*) $R = 19$; (*e*) $R = 6$; (*f*) $R = 2$; (*g*) $R = 1.01$.

as expected (cf. figure 12(*g*)), although the depth of the lower layer now adjusts smoothly to zero since there is a significant buoyancy contrast between the layers. As the viscosity of the upper layer increases, a larger fraction remains above the lower layer (figure 13(*e*, *f*)) and eventually, when $F^* = F = 1$, the upper layer remains above the lower layer at all points, and each current has the same depth (figure 13*d*). As the current passes through the point $RV = 1$, corresponding to $R^* \to \infty$, an inflection again develops in the upper layer.

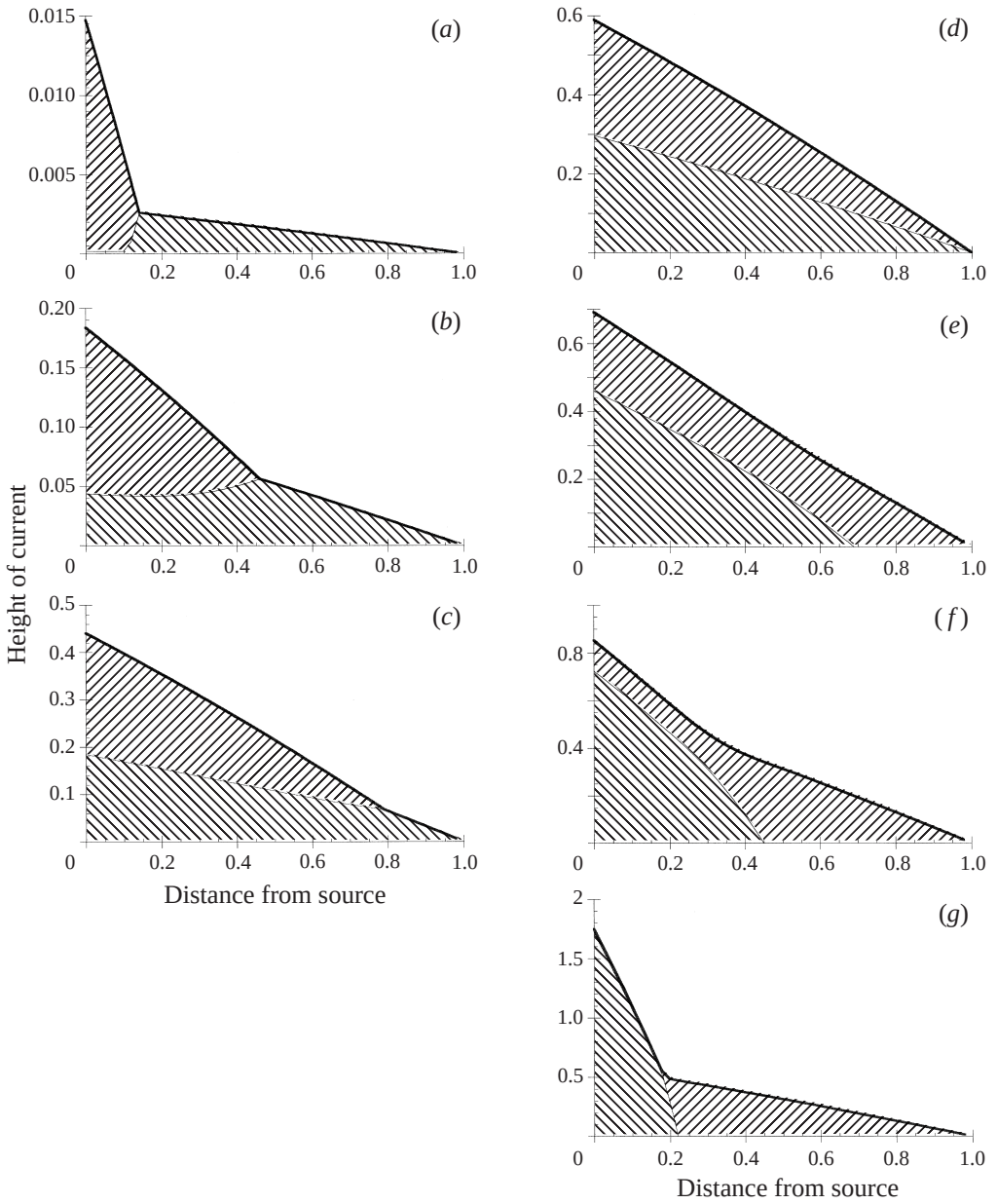

FIGURE 13. Variation of the flow morphology in a two-layer current produced by a maintained source of fluid as a function of the viscosity ratios. In all calculations the density ratio has value $R = 2$ and the flux ratio $F = 1$. The viscosity ratio takes the values (*a*) $V = 100$; (*b*) $V = 3$; (*c*) $V = 1$; (*d*) $V = 0.666$; (*e*) $V = 0.3$; (*f*) $V = 0.1$; (*g*) $V = 0.01$.

5.2. *Lower layer of greater extent, $\eta_l > \eta_u$*

A similar approach was used for the numerical solution in the case where the upper layer extends beyond the lower layer. Now, ζ is defined by

$$\zeta = \eta/\eta_l \tag{5.16}$$

and we set

$$(n_u, n_l) = \eta_l^2 (f_u, f_l). \tag{5.17}$$

At the leading edge of the current, $\zeta = 1$, we require

$$n_l(1) = 0 \quad \text{and} \quad \frac{\mathrm{d}n_l}{\mathrm{d}\zeta}(1-) = -\frac{2}{3RV} \tag{5.18}$$

while at the leading edge of the upper layer, $\zeta = \zeta_u = \eta_u/\eta_l$, we require

$$\frac{\mathrm{d}n_l}{\mathrm{d}\zeta}(\zeta_u+) = \frac{\mathrm{d}n_l}{\mathrm{d}\zeta}(\zeta-) + \frac{1}{R}\frac{\mathrm{d}n_u}{\mathrm{d}\zeta}(\zeta-) \tag{5.19}$$

and

$$\frac{\mathrm{d}n_u}{\mathrm{d}\zeta}(\zeta_u-) = \frac{1}{3}\left(-2\zeta_u + \frac{\mathrm{d}n_l}{\mathrm{d}\zeta}(\zeta_u-)\right). \tag{5.20}$$

The global mass conservation relations now become

$$\int_o^1 n_l \,\mathrm{d}\zeta = \eta_l^3 F \quad \text{and} \quad \int_0^{\zeta_u} n_u \,\mathrm{d}\zeta = \eta_l^3. \tag{5.21}$$

As in § 5.1, we integrate from the nose of the current backwards, and for each value of ζ_u we determine the corresponding value for F. In this way we may then determine solutions for given values of R, V and F.

Figure 12(*a–d*) illustrates the evolution of the shape of the current as the buoyancy ratio between the layers changes. The critical value $R = 19$, corresponding to the solution $F^* = F$ yields the solution $n_u = n_l$ as expected, since the difference in viscosity is exactly compensated by the contrast in buoyancy (figure 12*d*). As R increases, the lower layer begins to advance ahead of the upper layer (figure 12*b*, *c*) so that eventually most of the lower layer lies ahead of the upper layer (figure 12*a*). In this limit, in which $R = 1000$, the lower-layer buoyancy is so much larger than that of the upper layer, that it evolves almost independently of the upper layer. Furthermore, since the upper surface of the lower-layer current is of relatively shallow inclination, and the upper layer only covers the initial fraction of the lower layer, then the upper layer also evolves essentially independently of the lower layer. Note that in all these examples, $RV > 1$, and $V < 1$.

Figure 13(*a–d*) illustrates the evolution of the shape of the current as the viscosity ratio increases from the critical value for which $F^* = F$ (figure 13*d*). As the upper layer becomes relatively more viscous, it lags behind the lower layer (figure 13*b*, *c*), and as the current passes through the point $R = 1$, for which $F^* = 0$, the lower-layer depth actually begins to increase before reaching the leading edge of the upper layer (cf. § 3). In essence, the lower relatively dense and less-viscous layer squeezes out from under the upper layer, deepens, and then spreads into the region ahead of the upper layer (figure 13*a*). This behaviour contrasts with the case in which the lower layer is much denser, but more viscous than the upper layer (figure 12*a*). In that case the lower current behaves essentially independently of the upper layer.

6. Extension to continuously stratified fluid

The methodology presented above may be extended to describe multi-layer gravity-driven flows, although the algebra becomes increasingly involved. However, one natural limit concerns the evolution of a continuously stratified gravity current. Density-stratified currents can arise when fresh and brackish fluids mingle (e.g.

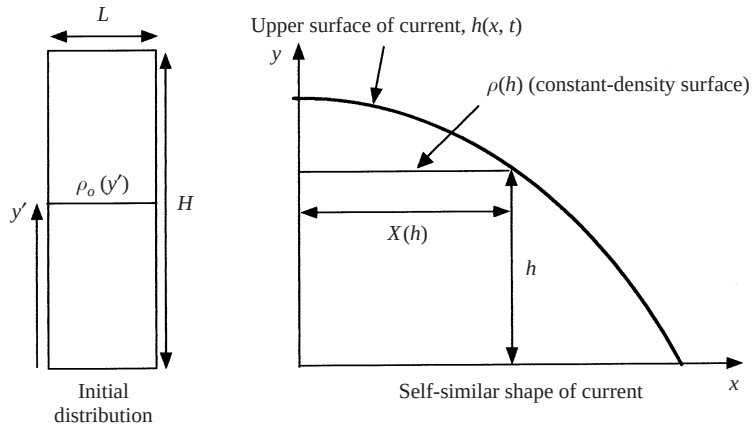

FIGURE 14. Schematic illustrating the structure of a density-stratified gravity current in a porous layer.

Phillips 1991). Viscosity-stratified currents may form during the secondary recovery of oil through liquid injection, if the concentration of polymer added to the injectate varies with time (Gorell & Homsy 1983; Manickam & Homsy 1993).

In general the evolution of a stratified current is complex since any shear in the current will lead to variations in the vertical density and viscosity profiles with lateral position in the current. However, two important cases involving a finite release of fluid are revealed by extension of the solutions described in § 3.

6.1. *Variable density, uniform viscosity*

In § 3.3.1, we showed that for a two-layer current in which each fluid has the same viscosity, $V = 1$, the depth of the lower layer remains constant until the depth of the upper layer falls to zero. By analogy, in the case of a density-stratified current of uniform viscosity we expect the density surfaces to be horizontal. As a result, the density gradient will vary with depth so as to conserve mass and buoyancy (figure 14). If we denote the upper surface of the current by $h(x,t)$, and the density at each height y to be $\rho + \Delta\rho(y,t)$, where ρ is a constant background value, then the pressure at some point (x,y) within the current is

$$p(x,y) = \int_y^{h(x,t)} g\Delta\rho(y,t)\,\mathrm{d}y + p_o(y), \tag{6.1}$$

where $p_o(y)$ is the background pressure. Therefore, applying Darcy's law and the local conservation of mass, we find (cf. (2.8))

$$\frac{\partial h}{\partial t} = \frac{kg}{\mu}\frac{\partial}{\partial x}\left(h\frac{\partial h}{\partial x}\Delta\rho(h,t)\right), \tag{6.2}$$

where for simplicity we consider the case $\phi = 1$.

For a finite release, equation (6.2) admits a self-similar solution of the form

$$h = A(\omega_s t)^{-1/3} f(\eta) \quad \text{and} \quad \eta = x/A(\omega_s t)^{1/3}, \tag{6.3}$$

where the reciprocal of the time scale, $\omega_s = kg\Delta\rho(0,0)/A\mu$, and where the constant A is determined in terms of the initial conditions as described below. In this self-similar

solution, we can express the current density as a function of the depth,

$$\Delta\rho(h,t) = \Delta\rho(0,0)b_s(f), \tag{6.4}$$

where $b_s(f)$ is a function to be found. Since $f(\eta)$, (6.3), is monotonic, we can also define the inverse function $\eta(f)$. Combining (6.2)–(6.4) we find that for a finite release

$$\frac{\mathrm{d}}{\mathrm{d}\eta}(\eta f) = -3\frac{\mathrm{d}}{\mathrm{d}\eta}\left(f\frac{\mathrm{d}f}{\mathrm{d}\eta}b_s(f)\right), \tag{6.5}$$

which admits solutions of the form

$$\eta = -3b_s(f)\frac{\mathrm{d}f}{\mathrm{d}\eta} \tag{6.6}$$

since $\mathrm{d}f/\mathrm{d}\eta = 0$ at $\eta = 0$.

We now show how to relate the initial fluid distribution to that of the self-similar flow described above. We suppose the current originates from a source reservoir of fluid, $0 < x < L$ and $0 < y' < H$, with initial density profile $\rho + \Delta\rho_o(y')$, where y' denotes the depth in the initial distribution (figure 14). Once the current has adjusted to the self-similar flow, with upper surface height $y = h(x,t)$ and density profile $\rho + \Delta\rho(y,t)$, where y is the vertical coordinate in the self-similar flow, then for $0 < y < h$, the conservation of volume requires

$$X(h,t)\,\mathrm{d}h = L\,\mathrm{d}y' \tag{6.7}$$

while the conservation of buoyancy requires

$$X(h,t)\Delta\rho(h,t)\,\mathrm{d}h = L\Delta\rho_o(y')\,\mathrm{d}y', \tag{6.8}$$

where $X(h,t)$ represents the lateral extent of the density surface at height h and y' is related to h according to $\Delta\rho(h,t) = \Delta\rho_o(y')$. Combining equations (6.7)–(6.8) with the above similarity solution, we find that

$$\eta(f)\frac{\mathrm{d}f}{\mathrm{d}y'} = \frac{L}{A^2} \tag{6.9}$$

and

$$\eta(f)b_s(f)\frac{\mathrm{d}f}{\mathrm{d}y'} = \frac{L}{A^2}\frac{\Delta\rho_o(y')}{\Delta\rho_o(0)}. \tag{6.10}$$

Combining (6.6) and (6.10) leads to the relation

$$-\eta^2\frac{\mathrm{d}\eta}{\mathrm{d}y'} = \frac{3L}{A^2}\frac{\Delta\rho_o(y')}{\Delta\rho_o(0)}. \tag{6.11}$$

Given the density distribution in the initial release of fluid, $\Delta\rho_o(y')$, we can then determine η as a function of y' and hence $f(\eta)$ and $b_s(f)$, (6.11), (6.6), (6.9), and the structure of the stratified current; in solving (6.11), we apply the boundary condition $\eta(y' = H) = 0$, and for convenience we choose $A^2 = LH$. We now consider an important specific example of the above general model.

6.1.1. *Uniformly stratified source fluid*

An important example concerns a linearly stratified source fluid,

$$\Delta\rho_o(y') = \Delta\rho_o(0)\frac{(H - y')}{H} \tag{6.12}$$

for which (6.11) gives the result

$$\eta_e^3 - \eta^3 = \frac{9L(2Hy' - y'^2)}{2HA^2}. \tag{6.13}$$

If we choose $A^2 = LH$ then

$$\frac{y'}{H} = 1 - \left(2\eta^3/9\right)^{1/2}, \tag{6.14}$$

where the condition $\eta(y' = H) = 0$ requires $\eta_e = (9/2)^{1/3}$. Since $b(f(\eta)) = 1 - y'/H$ we deduce that

$$b(f(\eta)) = \left(2\eta^3/9\right)^{1/2}. \tag{6.15}$$

From (6.6) we deduce that

$$f(\eta) = \frac{1}{3}\int_{\eta}^{\eta_e} \frac{\eta\,\mathrm{d}\eta}{\left(2\eta^3/9\right)^{1/2}} = \sqrt{2}((9/2)^{1/6} - \eta^{1/2}). \tag{6.16}$$

The density profile therefore has the form

$$b(f) = (1 - f/6^{1/3})^3 \tag{6.17}$$

in terms of the dimensionless height above the base of the layer. The functions (6.16) and (6.17) are shown in figure 15 for illustration.

6.2. *Variations in viscosity balancing variations in density*

By analogy with the case $F = F^*$ (§§ 3.1, 5.1), we expect that there is one particular relationship between density and viscosity for which the velocity of the current is independent of height and hence for which the vertical profiles of density and viscosity have the same form everywhere in the current.

If we denote the density, relative to the background, as a function of height by the relation

$$\Delta\rho(y) = \Delta\rho_o R(y/h), \tag{6.18}$$

where $h(x, t)$ is the depth of the current, then using the hydrostatic approximation, the pressure in the current is given by

$$P(x, y) = \Delta\rho_o g h \int_{\xi}^{1} R(\xi)\,\mathrm{d}\xi + p_o(y), \tag{6.19}$$

where $p_o(y)$ denotes the background pressure and here we set $\xi = y/h$. The speed in the current is therefore given by

$$u(x, \xi) = -\frac{kg\Delta\rho_o}{\mu(\xi)}\frac{\partial h}{\partial x}\int_{\xi}^{1} R(s)\,\mathrm{d}s \tag{6.20}$$

and the flux beneath the surface $y = \xi h(x, t)$ is

$$Q = \int_0^y u\,\mathrm{d}y = -k\Delta\rho_o g h\frac{\partial h}{\partial x}\int_0^{\xi}\mathrm{d}s\frac{1}{\mu(s)}\int_s^1 R(s')\,\mathrm{d}s'. \tag{6.21}$$

The rate of change of height of the density surface, $y = h_\rho(x, t) = \xi h$, with time is then given by

$$\frac{\partial h_\rho}{\partial t} = -\frac{\partial Q}{\partial x}. \tag{6.22}$$

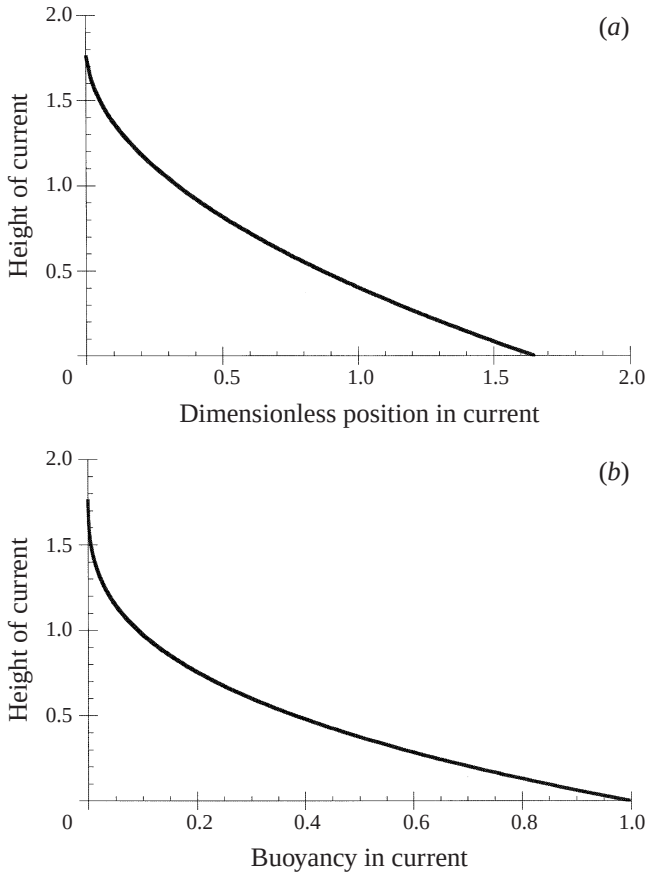

FIGURE 15. Dimensionless shape and buoyancy profile of a density-stratified gravity current produced from a discrete release of uniformly stratified fluid.

Combining (6.21) and (6.22), we find

$$\xi \frac{\partial h}{\partial t} = k\Delta\rho_o g \frac{\partial}{\partial x}\left(h\frac{\partial h}{\partial x}\right)\int_0^\xi \mathrm{d}s \frac{1}{\mu(s)}\int_s^1 R(s')\,\mathrm{d}s', \tag{6.23}$$

where we have used the constraint that ξ is independent of position in the current, and where for simplicity we set $\phi = 1$. Equation (6.23) holds for all values of ξ, and so

$$\xi = \beta \int_0^\xi \frac{\mathrm{d}s}{\mu(s)}\int_s^1 R(t)\,\mathrm{d}t, \tag{6.24}$$

where β is a constant determined below. Equation (6.24) is equivalent to the relation

$$\mu(\xi) = \beta \int_\xi^1 R(t)\,\mathrm{d}t. \tag{6.25}$$

6.2.1. *Uniform density with variation in viscosity*

A simple example of this class of flow concerns the gravitational spreading of fluid with a gradient of viscosity, but of uniform density, $\Delta\rho_o$, relative to the ambient, $R = 1$. For example, such a flow may develop if the mass of polymer mixed into fluid to be injected into a reservoir varies with time, as may occur in some enhanced oil

recovery schemes (Gorell & Homsy 1983). To achieve the particular self-similar flow for such a current, as described by (6.25), the viscosity profile should have the form

$$\mu(\xi) = \beta(1 - \xi) \tag{6.26}$$

and so β corresponds to the viscosity at the base of the flow. In this case, the current advances with a vertically uniform velocity, and each surface of constant viscosity, $\mu(\xi)$, is described by the classic parabolic solution (3.1), with the height scaled by the factor ξ ($0 < \xi < 1$). The current is able to advance in a self-similar fashion, with a uniform speed, since the hydrostatic pressure gradient increases with depth below the surface of the current at exactly the same rate as the viscosity.

7. Conclusions and discussion

We have examined the gravity-driven motion of two layers of fluid, of different viscosity and density, through a model porous layer. By developing a theoretical model, we have identified and calculated similarity solutions for both an instantaneous release of a finite mass of each fluid, and for a maintained release of each fluid. The models identify how the buoyancy and viscosity ratios of the layers control which of the two layers advances more rapidly. We show that if the contrast in viscosity and buoyancy of the two layers exactly compensate each other, $F = F^*$ (§§ 3.1, 5.1), then the current evolves as if it were a single layer of fluid; the velocity of each layer is the same and so the ratio of the depths of the two layers remains constant throughout the current.

For the case of a finite release of fluid, the changes in the structure of the current are most readily understood from figure 3 (§ 3.6). This figure illustrates that if the viscosity ratio of the upper- to lower-layer fluid is sufficiently large, $V > V_d$ ($F < F_d$), (3.46), then the lower-layer current detaches from the origin and advances ahead of the upper layer. For smaller viscosity ratios, $V_d > V > V^*$, the lower layer remains attached to the source, but still advances ahead of the upper layer. However, if V is smaller than the critical value V^* ((3.45), i.e. $F = F^*$), then the upper layer advances ahead of the lower layer. Finally, when the upper layer is of sufficiently low viscosity, $V < V_u$ ((3.47), i.e. $F > F_u$), it actually separates from the source. Equation (3.45) indicates that $V^* = 1$ in the limit $F \to 0$, so that the lower layer will only run ahead of a large volume of upper-layer fluid if it is less viscous; in contrast, when $F \to \infty$, $V^* = 1/R$, so that the upper layer will only run ahead of a large volume of lower-layer fluid if it has viscosity smaller than the density ratio. We note that for these finite currents, the shape of the upper surface of each layer is given analytically as a combination of parabolas. This provides a useful benchmark for numerical models of such flows.

We have also described a series of laboratory experiments using a Hele-Shaw cell to examine the propagation of such two-layer gravity currents. The experimental observations are in reasonable agreement with the similarity solutions. They also show that the flow rapidly evolves towards the self-similar form once the aspect ratio of the currents (height/length) has increased beyond about 1:10 (figures 6, 9).

Finally, we have extended the model to describe the propagation of density- and viscosity-stratified gravity currents. New classes of similarity solutions are presented to describe the spreading of (i) a finite release of density-stratified fluid of uniform viscosity, and (ii) a viscosity-stratified fluid of constant density. These solutions provide qualitative insight for the process of secondary oil recovery if the polymer concentration of liquid injected into the reservoir varies with time. However, further

analysis is required to model more general initial conditions and to account for the effects of capillarity and wetting.

Although the work is based on a simple, constant-permeability model of a porous layer, and does not account for effects of capillarity and non-uniformities in the structure of the rock, the models do provide fundamental insights into some aspects of the macroscopic behaviour of gravity- (rather than pressure-) driven flows, in particular, the prediction of which of the two layers advances furthest into the rock. Another key feature of the experiments is the absence of small-scale viscous fingering and the associated formation of an intermediate zone in which the two fluids are intermingled (Saffman & Taylor 1959; Chouke *et al.* 1959). Instead, after the initial transient, the pressure gradient, which is the result of gradients in the gravitational head, decreases in the direction of the flow, and the interface remains quite sharp, with the less-dense fluid lying above the denser layer (figures 6, 9).

Noting the simplifications, it is of interest to consider the implications of the model for displacement flows in porous rocks. First, we consider how a cloud of relatively dense pollutant, which has contaminated a porous layer, may be contained by injecting a volume of relatively light fluid laden with gel which is designed to set at some time after release. As a simplification we assume that up to the point of setting, the light fluid remains of uniform viscosity, but then it sets in place. The objective of the injection process is to contain the pollutant below the cloud of light injectate, so that when the gel sets, the pollutant remains confined (e.g. figure 2*a*, *b*; figure 6). We showed in § 2 that the relative motion of the pollutant and the light fluid depends on the viscosity ratio, the buoyancy ratio and the volume ratio. Equation (3.7) establishes the critical volume ratio at which the upper-layer fluid overruns the lower layer, and thereby can contain the contaminant. Equation (3.37) establishes the critical volume ratio at which the upper layer detaches from the source and hence at which the contaminant would become exposed at the source. The critical value of F has been plotted as a function of R in figure 16 for a viscosity ratio, $V = 0.1$. The plot identifies the important result that there is a range of buoyancy contrasts which will enable trapping of the contaminant. For smaller buoyancy contrast, the upper layer separates from the source, while for larger contrast, the lower layer runs under and ahead of the injected fluid. Similar principles apply for different viscosity contrasts, the key constraint being that the injected fluid is less viscous than the contaminant, otherwise the contaminant will run ahead of the injectate. The volume of injectate should also be comparable to the volume of contaminant in the rock, unless the viscosity and buoyancy ratios can be matched so that their product lies close to unity, in which case it would be possible to use less of the gelling injectate to trap the contaminant.

Second, we consider the injection of polymer-rich water into a reservoir to displace a finite layer of oil. Although this is a highly complex multiphase problem, in which both fluids may be stratified in viscosity and density, it is of interest to examine the qualitative type of flow which may develop in the two-layer gravity-dominated flow regime. We neglect the effects of capillary forces, wetting and the effects of any mixed zone which may develop in the vicinity of the displacing front, and which leads to a partially water- and partially oil-saturated zone (e.g. Lake 1989). The model predictions may be most applicable for flow in rock whose permeability is primarily associated with fractures. For typical density ratios $R \sim 1$–2 and viscosity ratios $V \sim 10$–1000, we expect that the water will advance below and ahead of the oil (figures 2*g*, *f*; figure 9), displacing relatively little oil per unit liquid injected. Again this flow may be interpreted as a single gravity-controlled viscous finger of water

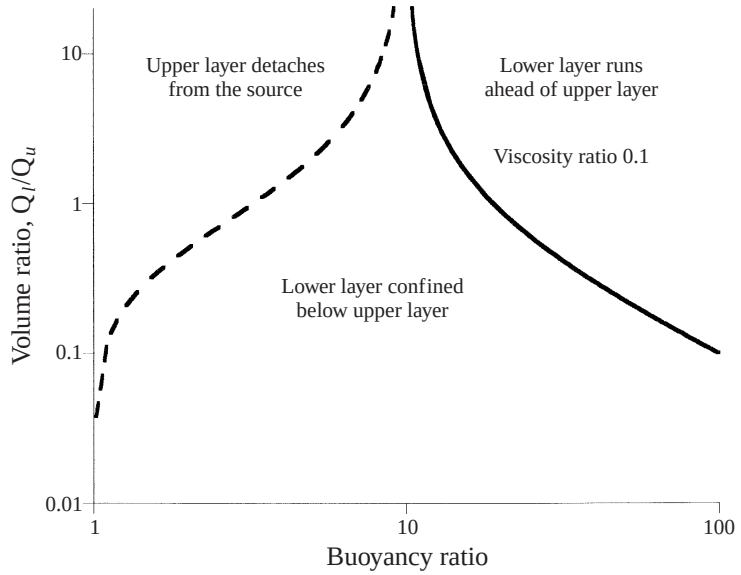

FIGURE 16. Illustration of the region in the volume ratio–buoyancy ratio space in which a light layer of fluid will act to confine a denser layer of fluid. Here the viscosity ratio $V = 0.1$.

running under the oil. In some cases, the viscosity of the injected water is increased by adding polymer. If the viscosity of the polymer-rich water were comparable to that of the oil, then from the results of § 3 we would expect that a larger mass of oil would be displaced per unit mass of water injected (figure 2*d*, *e*).

We are at present extending this work to include a number of additional processes which may influence the evolution of the system including wetting effects and the development of partially saturated zones. For immiscible displacements, capillary forces may act to change the structure of such gravity currents owing to retention of fluid in some of the pore spaces. Although this is a complex process, if the properties of the porous layer are uniform then, for the purposes of macroscopic modelling, one can model the action of surface tension on the drainage of the fluid by assuming that a uniform fraction of the fluid is retained as an interface recedes (cf. Barenblatt 1996; Woods 1998). The models presented above may be extended to describe this situation by using a differential form for global mass conservation which accounts for the loss of mass from the current (cf. Woods 1998). It would also be of interest to examine in more detail the initial transient adjustment of the currents towards the self-similar structure. During the early stages when the flow is dominated by the applied pressure, the two fluids mingle within the pore spaces and a morphologically complex two-phase flow develops, with the pore space being partially saturated in each fluid phase. This contrasts with the simpler interface morphology which we have examined and illustrated experimentally in a Hele-Shaw cell when the dynamics is dominated by gravity. The models may be extended to describe radially symmetric displacement flows (cf. Woods 1998), and although beyond the scope of the present study, in that case, the gravitational forces will become increasingly dominant relative to the applied pressure forces with distance from the source.

Finally, we mention that the insight developed from this study provides new understanding of the propagation of gravity-driven reaction fronts. Such fronts may be produced when a reactant-laden fluid migrates under gravity through a permeable

rock (Phillips 1991). In that case, the regions ahead of and behind the reaction front are of different permeability and porosity. This has some analogy with the propagation of a two-layer gravity current in which the layers have different viscosity; indeed, many features of the flow and reaction patterns may be understood by reference to the present work (Raw & Woods 2000).

REFERENCES

Barenblatt, G. 1996 *Scaling, Self-similarity and Intermediate Asymptotics*. Cambridge University Press.

Bear, J. 1972 *Dynamics of Flow in Porous Media*. Elsevier.

Chouke, R. L., Meurs, P. & Poel, C. van der 1959 The instability of slow immiscible, viscous liquid–liquid displacement in permeable media. *Trans. AIME* **216**, 188–194.

Dullien, F. A. L. 1992 *Porous Media – Fluid Transport and Pore Structure*. Academic.

Gorell, S. & Homsy, G. 1983 A theory of optimal policy of oil recovery by secondary displacement processes. *SIAM J. Appl. Maths* **43**, 79–98.

Homsy, G. M. 1987 Viscous fingering in porous media. *Ann. Rev. Fluid Mech.* **19**, 271–311.

Huppert, H. E. 1986 The intrusion of fluid mechanics into geology. *J. Fluid Mech.* **173**, 557–594.

Huppert, H. E. & Woods, A. W. 1995 On gravity driven flows in a porous medium. *J. Fluid Mech.* **292**, 52–69.

Lake, L. 1989 *Enhanced Oil Recovery*. Prentice Hall.

Manickam, O. & Homsy, G. M. 1993 Stability of miscible displacements in porous media with nonmonotonic viscosity profiles. *Phys Fluids* A **5**, 1356–1367.

Pattle, R. E. 1959 Diffusion from an instantaneous source with a concentration dependent diffusivity. *Q. J. Mech. Appl. Maths* **12**, 407–409.

Peters, B. M., Zhou, D. & Blunt, M. 1997 Experimental investigation of scaling factors that describe miscible floods in layered systems. *SPE Paper* 39624, pp. 1–8.

Phillips, O. M. 1991 *Flow and Reactions in Permeable Rock*. Cambridge University Press.

Raw, A. & Woods, A. W. 2000 The dynamics of gravity driven reaction fronts in a porous layer. *Stanford Geothermal Workshop*. Stanford University Press.

Saffman, P. G. & Taylor, G. I. 1958 The penetration of a fluid into a porous medium or Hele-Shaw cell containing a more viscous liquid. *Proc. R. Soc. Lond.* A **245**, 312–329.

Tchelepi, H. A. & Orr, F. M. 1993 The interaction of viscous fingering, permeability heterogeneity and gravity in 3-D. *SPE Paper* 27834.

Woods, A. W. 1998 Vaporising gravity currents in a permeable rock. *J. Fluid Mech.* **377**, 151–168.

Woods, A. W. 1999 Liquid and vapor flow in superheated rock. *Ann. Rev. Fluid Mech.* **31**, 171–199.

Zhou, D. & Blunt, M. 1997 Effect of spreading coefficient on the distribution of light non-aqueous phase liquid in the subsurface. *J. Contaminant Hydrol.* **25**, 1–19.

Zimmerman, W. B. & Homsy, G. M. 1991 Nonlinear viscous fingering in miscible displacement with anisotropic dispersion. *Phys Fluids* A **3**, 1859–1872.